ROMAI J., v.18, no.1(2022), 31–73

EFFICIENT SOLVERS FOR NONSTANDARD MODELS FOR FLOW AND TRANSPORT IN UNSATURATED POROUS MEDIA

Davide Illiano[1], Jakub Wiktor Both[2], Iuliu Sorin Pop[3], Florin Adrian Radu[2]
[1] *NORCE Norwegian Research Center, Bergen, Norway,*
[2] *Center for Modeling of Coupled Subsurface Dynamics, Department of Mathematics, University of Bergen, Norway,*
[3] *Hasselt University, Hasselt, Belgium*
davide.illiano@norce.no florin.radu@uib.no, jakub.both@uib.no,sorin.pop@uhasselt.be

Abstract We study several iterative methods for fully coupled flow and reactive transport in porous media. The resulting mathematical model is a coupled, nonlinear evolution system. The flow model component builds on the Richards equation, modified to incorporate nonstandard effects like dynamic capillarity and hysteresis, and a reactive transport equation for the solute. The two model components are strongly coupled. On one hand, the flow affects the concentration of the solute; on the other hand, the surface tension is a function of the solute, which impacts the capillary pressure and, consequently, the flow. After applying an Euler implicit scheme, we consider a set of iterative linearization schemes to solve the resulting nonlinear equations, including both monolithic and two splitting strategies. The latter include a canonical nonlinear splitting and an alternate linearized splitting, which appears to be overall faster in terms of numbers of iterations, based on our numerical studies. The (time discrete) system being nonlinear, we investigate different linearization methods. We consider the linearly convergent L-scheme, which converges unconditionally, and the Newton method, converging quadratically but subject to restrictions on the initial guess. Whenever hysteresis effects are included, the Newton method fails to converge. The L-scheme converges; nevertheless, it may require many iterations. This aspect is improved by using the Anderson acceleration. A thorough comparison of the different solving strategies is presented in five numerical examples, implemented in MRST, a toolbox based on MATLAB.

Keywords: flow and reactive transport in porous media, dynamic capillarity, hysteresis, Richards equation, Euler implicit scheme, L-scheme, Anderson acceleration
2010 MSC: 65N22, 65N30.

1. INTRODUCTION

Mathematical models for complex physical phenomena are generally neglecting several processes, in order to guarantee that the result is sufficiently simple and to facilitate the numerical simulations. With a particular focus

on porous media applications, in this sense we mention enhanced oil recovery, diffusion of substances in living tissues, and pollution of underground aquifers. With the increase of computational power, and the development of efficient simulation algorithms, mathematical models are improved continuously, and more and more of the neglected effects are included.

When studying unsaturated flow, the equilibrium capillary pressure plays a fundamental role. It is typically assumed to be a nonlinear, monotone function of the water content. Explicit representations have been obtained thanks to numerous experiments under equilibrium conditions (no flowing phases). Even though this formulation has been the most commonly used in the last decades, it has been observed [18, 25, 53, 65], that changes in time of the water content, thus its time derivatives, do influence the profile of the capillary pressure. In terms of modeling, this is achieved by including the so-called dynamic effects [13, 30, 47]. Numerous papers investigate the existence of a solution for systems including such effects, among them we cite [20, 41, 48]. Furthermore, the problem has been already studied numerically in, e.g., [2, 3, 21].

The hysteresis effect is another phenomenon often neglected. Again, experiments have revealed that the curve obtained when investigating the imbibition process, is different from the one observed during the drainage, [23, 34, 50, 51]. This is sketched in Fig. 1.

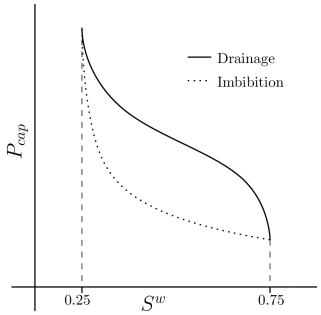

Fig. 1.: Primary hysteresis loop as presented in [50].

In this article, we study unsaturated flow in porous media, modeled by the Richards equation [14, 32], however including both dynamic and hysteresis effects. Furthermore, we include a solute component, e.g., a surfactant, in the wetting phase, which can directly influence the fluid properties ([4, 56]). The study of the transportation of an external components, e.g., surfactant, in variably saturated porous media has been already investigated both numerically [36, 42, 59] and experimentally [33, 38].

Here, we will mainly concentrate on numerical studies, extending the solution techniques in [36] to include dynamic capillarity and hysteresis We con-

sider the following model for coupled unsaturated flow and reactive transport

$$\begin{aligned} \partial_t \theta(\Psi, c) - \nabla \cdot (K(\theta(\Psi, c)) \nabla(\Psi + z)) &= \mathbb{S}_1, \\ \partial_t (\theta(\Psi, c) c) - \nabla \cdot (D \nabla c - \mathbf{u_w} \mathbf{c}) + \mathbf{R}(\mathbf{c}) &= \mathbb{S}_\mathbf{2}. \end{aligned} \tag{1}$$

Here, $\theta(\Psi, c)$ is the water content, expressed as a function of both the unknown pressure head Ψ and the concentration of the external component c. K, a function of the water content θ, is the conductivity, z the vertical coordinate of $\vec{x}$, pointing against gravity, D the dispersion/diffusion coefficient, $\mathbf{u_w} := -\mathbf{K}(\boldsymbol{\theta}(\boldsymbol{\Psi}, \mathbf{c}))\boldsymbol{\nabla}(\boldsymbol{\Psi} + \mathbf{z})$ the water flux, $R(c)$ the reaction term and $\mathbb{S}_1, \mathbb{S}_2$ the external sink/source terms involved.

Next to a concentration dependence of θ and Ψ, here we include also play-type hysteresis and dynamic capillary effects as introduced in [13]. More precisely,

$$\Psi \in -p_{cap}(\theta, c) + \tau(\theta) \partial_t \theta + \gamma(\theta) \operatorname{sign}(\partial_t \theta), \tag{2}$$

where p_{cap} is the equilibrium capillary pressure, expressed as a function of θ and c, $\tau(\theta)$ the dynamic effects, and $\gamma(\theta)$ the width of the primary hysteresis loop. Later on, for ease of presentation, we consider γ as a positive constant, $\gamma \in \mathbb{R}_{\geq 0}$. Note that (2) is a differential inclusion as the sign graph is multi-valued and defined as follow,

$$sign(\xi) = \begin{cases} 1 & \text{for } \xi > 0, \\ [-1, 1] & \text{for } \xi = 0, \\ -1 & \text{for } \xi < 0. \end{cases} \tag{3}$$

The multi-valued graph allows switching between the imbibition and drainage curves in the play-type hysteresis. For more details on the formulation we refer to [13].

The primary unknowns of the system are the pressure Ψ, the concentration c and the water content θ. In standard models, also obtained as special case for $\gamma = \tau(\theta) = 0$, θ is a function of pressure and concentration. Therefore, (2) is replaced by an algebraic relationship, which simplifies the model and allows eliminating θ as an unknown. In the extended/nonstandard formulation, θ is an unknown and (2) is required as additional equation of the model. Initial and boundary conditions will complete the system.

To avoid working with a graph, we consider the following regularization,

$$\Phi(\xi) = \begin{cases} \operatorname{sign}(\xi) & \text{if} \quad |\xi| \geq \delta, \\ \frac{\xi}{\delta} & \text{if} \quad |\xi| < \delta, \end{cases} \tag{4}$$

where $\delta \in \mathbb{R}^+$ is a small parameter. Using this in (2) gives the regularized system of equations

$$\begin{aligned} \partial_t \theta - \nabla \cdot (K(\theta)\nabla(\Psi + z)) &= \mathbb{S}_1, \\ \Psi = -p_{cap}(\theta, c) + \tau(\theta)\partial_t \theta + \gamma\Phi(\partial_t \theta), \\ \partial_t(\theta c) - \nabla \cdot (D\nabla c - \mathbf{u_w c}) + \mathbf{R}(\mathbf{c}) &= \mathbb{S}_2. \end{aligned} \tag{5}$$

From now on, the system (5) will be further investigated. We will discretize the equations and study different solving algorithms.

Remark 1.1. *An inverse formulation is proposed in [13], obtained by solving* (2)*, as its regularized counterpart in* (5)*, in terms of* $\partial_t \theta$*. This gives*

$$\partial_t \theta = F(\Psi, \theta, c), \tag{6}$$

for a suitable function F*. The time derivative in the flow equation can then be substituted by* F*,*

$$F(\Psi, \theta, c) - \nabla \cdot \big(K(\theta)\nabla(\Psi + z)\big) = \mathbb{S}_1. \tag{7}$$

This formulation is used for the mathematical analysis of such models, [19, 61]. It has been observed, e.g., in [46], that such formulation can reduce the number of iterations required to solve the system of equations, compared to the formulation in (2)*. However, for the particular test cases investigated here, no remarkable improvements are observed. Thus, for ease of presentation, we will report the results obtained only for the formulation given by (5).*

We point out that the concentration of the external component directly influences the capillary pressure. The presence of such a component results in a non-constant surface tension, which induces a rescaling of the pressures [35, 63, 64].

To solve the system (5) numerically, one first needs to discretize in time and space, and then develop solvers for the discretized equations. In this paper, due to the expected low regularity of the solutions [6] and the desire of relatively large time steps, we choose to use the backward Euler method for the time discretization. Certain processes investigated in porous media flow can take place on time intervals longer than decades, thus the need for large time steps. Multiple spatial discretization techniques are available, e.g., the Galerkin Finite Element Method (*FEM*) [11, 52, 60], Discontinuous Galerkin Method (*DGM*) [9, 39, 43, 66], the Mixed Finite Element Method (*MFEM*) [8, 21, 58, 59, 67, 70], the Finite Volume Method (*FVM*) [27] and the Multi-Point Flux Approximation (*MPFA*) [1, 10, 12, 40]. We will here concentrate on *FEM* and *TPFA* (Two Points Flux Approximation), a particular case of *MPFA*. In particular, we cite [15, 26, 71] for papers on improved numerical schemes applied to the Richards equation.

Since the equations investigated here are characterized by several nonlinear quantities, $K(\theta)$, $p_{cap}(\theta, c)$, $\tau(\partial_t \theta)$, and $R(c)$, and the time discretization is not explicit, one needs to solve a nonlinear system at each time step, requiring a linearization procedure. Examples of possible linearization schemes are: the Newton method [54], the modified Picard method [24] and the L-scheme [45, 57]. In this paper, we investigate the Newton method and the L-scheme. The former is a commonly used linearization scheme which is quadratically convergent. However, this convergence is only local and one needs to compute the Jacobian matrix, which can be expensive. The L-scheme is instead globally (linearly) convergent, under mild restrictions, and it does not require the computation of any derivative. The L-scheme is in general slower in terms of numbers of iterations than the Newton method. Moreover, the linear systems to be solved within each iteration are better conditioned when compared to the ones given by the Newton method [36, 45]. Furthermore, the rate of convergence of the scheme strongly depends on user-defined parameters. Such aspects are investigated for numerous nonlinear problems, including Richards equation, and two-phase flow in porous media, in [36, 45, 49, 57, 62]. Finally there numerous papers proposing improved formulation of the L-scheme, among them we cite [5, 49].

In this work, we test the L-scheme on more complex problems involving hysteresis and dynamic effects, and coupled reactive transport and flow. Furthermore, we investigate a post-processing technique, the Anderson Acceleration (AA) [7], which can drastically improve linearly convergent schemes. The acceleration tool requires user-defined parameters. As will be seen below, choosing the suitable parameters for the AA, significantly relaxes the choice of the parameters for the L-scheme linearization.

We observe that the system (5) is fully coupled. This is due to the dependence of the capillary pressure on both θ and c. Therefore, we will investigate multiple solution algorithms, combining different linearization schemes and decoupling techniques. Decoupling/splitting the equations may present multiple advantages such as: an easier implementation, a better conditioned problem to solve, similar convergence properties but faster computations. We divide the schemes into three main categories: monolithic (Mono), nonlinear splitting (NonLinS) and alternate splitting (AltS). Subsequently, we denote, e.g., by Newton-Mono, the monolithic scheme obtained by applying the Newton method as linearization. Such schemes have already been investigated for the standard model in [36].

The paper is organized as follows. In Section 2, we present the linearization and discretization techniques including monolithic or decoupled solution approaches. Section 3 presents five different numerical examples, which allow to compare the efficiency and robustness of the solving algorithms. Section 4 concludes this work with the final remarks.

2. PROBLEM FORMULATION, DISCRETIZATION AND ITERATIVE SCHEMES

In the following, we use the standard notations of functional analysis. The domain $\Omega \subset \mathbb{R}^d$, $d = 1, 2$ or 3, is bounded and has a Lipschitz continuous boundary $\partial\Omega$. The final time is $T > 0$, and the time domain is $(0, T]$. $L^2(\Omega)$ denotes the space of real valued, square integrable functions defined on Ω and $H^1(\Omega)$ its subspace containing the functions also having weak first derivatives in $L^2(\Omega)$. $H_0^1(\Omega)$ is the space of functions belonging to $H^1(\Omega)$, having zero trace on the boundary $\partial\Omega$. Furthermore, we denote by $< \cdot, \cdot >$ the standard $L^2(\Omega)$ scalar product and by $\|\cdot\|$ the associated norm.

To numerically solve the system of equations (5), one needs to discretize both in time and space. We combine the backward Euler method with linear Galerkin finite elements. Let $N \in \mathbb{N}$ be a strictly positive natural number. We define the time step size $\Delta t = T/N$ and $t_n = n\Delta t$ $(n \in 1, 2, \ldots, N)$. Furthermore, let T_h be a regular decomposition of Ω, $\overline{\Omega} = \underset{T \in T_h}{\cup} T$, with h denoting the mesh diameter. The finite element spaces $V_h \subset H_0^1(\Omega)$ and $W_h \subset L^2(\Omega)$ are defined by

$$\begin{aligned} V_h &:= \left\{ v_h \in H_0^1(\Omega) \ s.t. \ v_{h|T} \in \mathbb{P}_1(T), \ T \in T_h \right\}, \\ W_h &:= \left\{ w_h \in L^2(\Omega) \ s.t. \ w_{h|T} \in \mathbb{P}_1(T), \ T \in T_h \right\}, \end{aligned} \tag{8}$$

where $\mathbb{P}_1(T)$ denotes the space of the linear polynomials on T. The fully discrete Galerkin formulation of the system (5) can now be written as:

Problem Pn: Let $n \geq 1$ be fixed. Assuming that $\Psi_h^{n-1}, c_h^{n-1} \in V_h$ and $\theta_h^{n-1} \in W_h$ are given, find $\Psi_h^n, c_h^n \in V_h$ and $\theta_h^n \in W_h$ such that

$$\begin{aligned} < \theta_h^n - \theta_h^{n-1}, v_{1,h} > + \Delta t < K(\theta_h^n)(\nabla \Psi_h^n + \mathbf{e_z}), \nabla v_{1,h} > \\ = \ \Delta t < \mathbb{S}_1, v_{1,h} > \\ \Delta t < \Psi_h^n, w_{1,h} > + \Delta t < p_{cap}(\theta_h^n, c_h^n), w_{1,h} > \\ - < \tau(\theta_h^n)(\theta_h^n - \theta_h^{n-1}), w_{1,h} > \ = \ \Delta t \gamma < \Phi \left(\frac{\theta_h^n - \theta_h^{n-1}}{\Delta t} \right), w_{1,h} > \\ < \theta_h^n (c_h^n - c_h^{n-1}) + c_h^n (\theta_h^n - \theta_h^{n-1}), v_{2,h} > + \Delta t < D \nabla \Psi_h^n \\ + \mathbf{u_w^n c_h^n}, \boldsymbol{\nabla} \mathbf{v_{2,h}} > + \boldsymbol{\Delta} \mathbf{t} < \mathbf{R}(\mathbf{c_h^n}), \mathbf{v_{2,h}} > \ = \ \Delta t < \mathbb{S}_2, v_{2,h} > \end{aligned} \tag{9}$$

holds for all $v_{1,h}, v_{2,h} \in V_h$ and for all $w_{1,h} \in W_h$. We denote by $\mathbf{e_z}$ the unit vector in the direction opposite to gravity.

Observe that choosing the space $H_0^1(\Omega)$ implies that homogeneous boundary conditions have been adopted for the pressure and the concentration. However, this choice is made for the ease of presentation, the extension to other

boundary conditions being possible without major complications. We also mention that, for $n = 1$, we use the approximation in V_h of the initial water content and concentration, respectively θ_h^0 and c_h^0.

In the following, we investigate different iterative schemes for solving Problem Pn. These schemes are based on the ones discussed in [36], extending them, not only to the case of dynamic capillary pressure ($\tau(\theta) \neq 0$) [37], but also to the case of hysteresis. Among the numerous papers investigating numerically the effects of hysteresis and dynamic capillarity pressure, we cite [55, 72]. As mentioned, we compare monolithic (Mono) and splitting (NonLinS and AltS) solvers, combined with two different linearization schemes, the Newton method and the L-scheme. Furthermore, the Anderson acceleration [7] will be taken into account to speed up the linearly convergent L-scheme.

2.1. SOLVING ALGORITHMS

In what follows, when solving (9) iteratively, the index n will always refer to the time step level, whereas j will denote the iteration index. As a rule, the iterations will start with the solution at the last time step, t_{n-1}, for example $\Psi^{n,1} = \Psi^{n-1}$. As mentioned, this choice is not required for L-type schemes but it is a natural one.

In a compact form Problem Pn can be seen as the system

$$\begin{cases} F_1(\Psi_h^n, \theta_h^n) & = 0, \\ F_2(\Psi_h^n, \theta_h^n, c_h^n) & = 0, \\ F_3(\Psi_h^n, \theta_h^n, c_h^n) & = 0, \end{cases} \tag{10}$$

with F_1, F_2 resulting from the flow equations and F_3 from the transport. In the following we will indicate with F^{lin}, the linearized formulation of F obtained by either the Newton method or the L-scheme. Finally, we can proceed to present monolithic and splitting solvers.

In the monolithic approach one solves the three equations of the system (10) at once. Formally, one iteration is:
Find $\Psi_h^{n,j+1}$, $\theta_h^{n,j+1}$ and $c_h^{n,j+1}$ such that

$$\begin{cases} F_1^{lin}(\Psi_h^{n,j+1}, \theta_h^{n,j+1}) & = 0, \\ F_2^{lin}(\Psi_h^{n,j+1}, \theta_h^{n,j+1}, c_h^{n,j+1}) & = 0, \\ F_3^{lin}(\Psi_h^{n,j+1}, \theta_h^{n,j+1}, c_h^{n,j+1}) & = 0, \end{cases} \tag{11}$$

where F_i^{Lin} is the linearization of F_i, $i \in \{1, 2, 3\}$. Depending on which linearization technique is used, we refer to the Newton-monolithic scheme (Newton-Mono) or monolithic-L-scheme (LS-Mono). These two schemes will be presented in details below. Fig. 2 displays the sketched version of the monolithic solver.

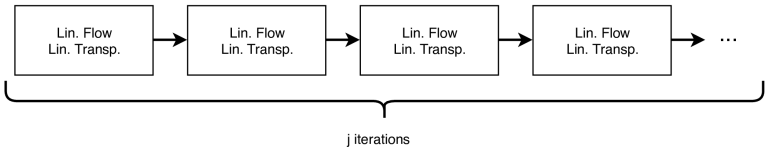

Fig. 2.: The monolithic approach.

In the iterative splitting approach, the flow and the transport equations are solved subsequently, iterating between them. We will distinguish between two primary splitting schemes: the nonlinear splitting (NonLinS) and the alternate linearized splitting (AltLinS), illustrated in Figure 3 and Figure 4, respectively. Such schemes have already been studied, in the case of a standard flow model in [36].
In the nonlinear splitting, one iteration step is:
Find first $\Psi_h^{n,j+1}$, $\theta_h^{n,j+1}$ such that

$$\begin{cases} F_1(\Psi_h^{n,j+1}, \theta_h^{n,j+1}) & = 0, \\ F_2(\Psi_h^{n,j+1}, \theta_h^{n,j+1}, c_h^{n,j}) & = 0, \end{cases} \tag{12}$$

and then find $c_h^{n,j+1}$ such that

$$F_3(\Psi_h^{n,j+1}, \theta_h^{n,j+1}, c_h^{n,j+1}) = 0. \tag{13}$$

The two flow equations are solved at once. Each of the nonlinear systems (12) and (13) is solved until some convergence criterion is met. Once the pressure and water content are obtained, $\Psi_h^{n,j+1}$ and $\theta_h^{n,j+1}$, are then used in the transport equation (13) to compute $c_h^{n,j+1}$. The resulting F_1, F_2 and F_3, being nonlinear, are linearized using the Newton method or the L-scheme.

In contrast, the alternate linearized splitting (AltLinS) schemes perform only one linearization step per iteration, see Figure 4. One iteration in the alternate splitting scheme can be written as:
Find $\Psi_h^{n,j+1}, \theta_h^{n,j+1}$ such that

$$\begin{cases} F_1^{lin}(\Psi_h^{n,j+1}, \theta_h^{n,j+1}) & = 0, \\ F_2^{lin}(\Psi_h^{n,j+1}, \theta_h^{n,j+1}, c_h^{n,j}) & = 0, \end{cases} \tag{14}$$

and then $c_h^{n,j+1}$ such that

$$F_3^{lin}(\Psi_h^{n,j+1}, \theta_h^{n,j+1}, c_h^{n,j+1}) = 0. \tag{15}$$

Again, depending on which linearization is used, we refer to alternate splitting Newton (AltS-Newton) or alternate splitting L-scheme (AltS-LS). Both schemes will be presented in detail below.

In the following sections we will illustrate, in the details, the different schemes here investigated.

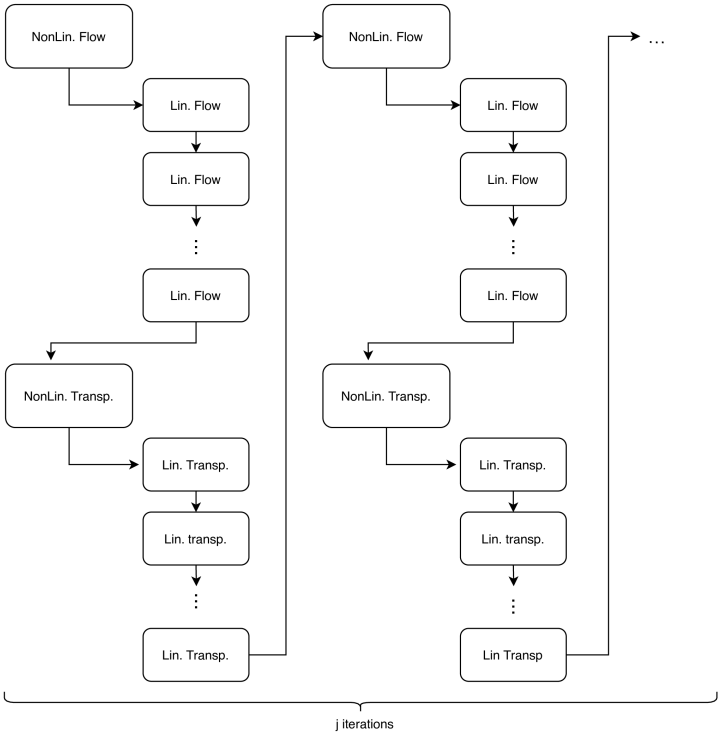

Fig. 3.: The nonlinear splitting approach.

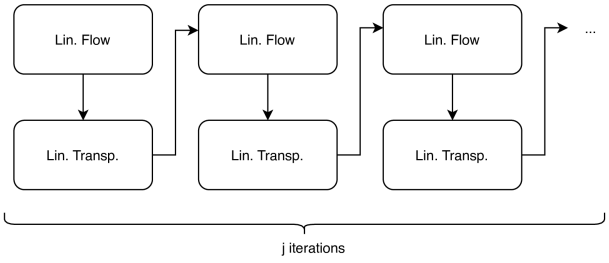

Fig. 4.: The alternate splitting approach.

2.1.1 The monolithic Newton method (Newton-Mono). The standard monolithic Newton method applied to (9) reads as:

Problem P-Newton-Mono: Let $j > 1$ be fixed. Let $\Psi_h^{n-1}, \Psi_h^{n,j}, c_h^{n-1}, c_h^{n,j} \in V_h$, and $\theta_h^{n-1}, \theta_h^{n,j} \in W_h$ be given, find $\Psi_h^{n,j+1}, c_h^{n,j+1} \in V_h$, and $\theta_h^{n,j+1} \in W_h$ such that

$$\begin{aligned} &< \theta_h^{n,j+1} - \theta_h^{n-1}, v_{1,h} > + \Delta t < K(\theta_h^{n,j})(\nabla(\Psi_h^{n,j+1}) + \mathbf{e_z}), \boldsymbol{\nabla} \mathbf{v_{1,h}} > \\ + \Delta t \quad &< \partial_\theta K(\theta_h^{n,j})(\nabla(\Psi_h^{n,j}) + \mathbf{e_z})(\boldsymbol{\theta}_\mathbf{h}^{\mathbf{n,j+1}} - \boldsymbol{\theta}_\mathbf{h}^{\mathbf{n,j}}), \boldsymbol{\nabla} \mathbf{v_{1,h}} > = \boldsymbol{\Delta} \mathbf{t} < \mathbb{S}_\mathbf{1}, \mathbf{v_{1,h}} > \end{aligned} \tag{16}$$

$$\begin{aligned} \Delta t < \Psi_h^{n,j+1}, w_{1,h} > \quad &= -\Delta t < p_{cap}(\theta_h^{n,j}, c_h^{n,j}), w_{1,h} > - \\ &-\Delta t < \partial_\theta p_{cap}(\theta_h^{n,j}, c_h^{n,j})(\theta_h^{n,j+1} - \theta_h^{n,j}), w_{1,h} > \\ &-\Delta t < \partial_c p_{cap}(\theta_h^{n,j}, c_h^{n,j})(c_h^{n,j+1} - c_h^{n,j}), w_{1,h} > + \\ &+ < \tau(\theta_h^{n,j})(\theta_h^{n,j+1} - \theta_h^{n-1}), w_{1,h} > + \\ &+ < \partial_\theta \tau(\theta_h^{n,j})(\theta_h^{n,j} - \theta_h^{n-1})(\theta_h^{n,j+1} - \theta_h^{n,j}), w_{1,h} > + \\ &+ \Delta t \gamma < \Phi\left(\tfrac{\theta_h^{n,j} - \theta_h^{n-1}}{\Delta t}\right), w_{1,h} > \end{aligned} \tag{17}$$

and

$$\begin{aligned} < \theta_h^{n,j}(c_h^{n,j+1} - c_h^{n-1}) + c_h^{n,j}(\theta_h^{n,j+1} - \theta_h^{n-1}), v_{2,h} > + \\ + \Delta t < D \nabla c_h^{n,j+1} + \mathbf{u}_w^{n,j} c_h^{n,j+1}, \nabla v_{2,h} > + \\ + \Delta t < R(c_h^{n,j}), v_{2,h} > + \\ + \Delta t < \partial_c R(c_h^{n,j})(c_h^{n,j+1} - c_h^{n,j}) > \quad = \Delta t < \mathbb{S}_2, v_{2,h} > \end{aligned} \tag{18}$$

hold true for all $v_{1,h}, v_{2,h} \in V_h$, and for all $w_{1,h} \in W_h$. By ∂_θ we denote the partial derivative with respect to the water content θ, and by ∂_c the partial derivative with respect to the concentration c, and $\mathbf{u}_w^{n,j} := -K(\theta_h^{n,j})\nabla(\Psi_h^{n,j} + \mathbf{e_z})$.

2.1.2 The monolithic *L*-scheme (LS-Mono).

The monolithic L-scheme for solving (9) reads:

Problem P-LS-Mono: Let $j > 1$ be fixed. Let $\Psi_h^{n-1}, \Psi_h^{n,j}, c_h^{n-1}, c_h^{n,j} \in V_h$, and $\theta_h^{n-1}, \theta_h^{n,j} \in W_h$ be given, find $\Psi_h^{n,j+1}, c_h^{n,j+1} \in V_h$, and $\theta_h^{n,j+1} \in W_h$ such that

$$\begin{aligned} < \theta_h^{n,j+1} - \theta_h^{n-1}, v_{1,h} > + \\ \Delta t < K(\theta_h^{n,j})(\nabla(\Psi_h^{n,j+1}) + \mathbf{e}_z), \nabla v_{1,h} > + \\ + L_1 < \Psi_h^{n,j+1} - \Psi_h^{n,j}, v_{1,h} > \quad = \Delta t < \mathbb{S}_1, v_{1,h} > \end{aligned} \tag{19}$$

$$\begin{aligned}\Delta t < \Psi_h^{n,j+1}, w_{1,h} >= \quad & -\Delta t < p_{cap}(\theta_h^{n,j}, c_h^{n,j}), w_{1,h} > + \\ & + < \tau(\theta_h^{n,j})(\theta_h^{n,j+1} - \theta_h^{n-1}), w_{1,h} > + \\ & + \Delta t\gamma < \Phi\left(\tfrac{\theta_h^{n,j} - \theta_h^{n-1}}{\Delta t}\right), w_{1,h} > + \\ & + L_2 < (\theta_h^{n,j+1} - \theta_h^{n,j}), w_{1,h} >\end{aligned} \tag{20}$$

and

$$\begin{aligned}< \theta_h^{n,j}(c_h^{n,j+1} - c_h^{n-1}) + c_h^{n,j}(\theta_h^{n,j+1} - \theta_h^{n-1}), v_{2,h} > + \\ + \Delta t < D\nabla c_h^{n,j+1} + \mathbf{u}_w^{n,j} c_h^{n,j+1}, \nabla v_{2,h} > + \\ + \Delta t < R(c_h^{n,j}), v_{2,h} > + L_3 < c_h^{n,j+1} - c_h^{n,j}, v_{2,h} > \quad = \Delta t < \mathbb{S}_2, v_{2,h} >\end{aligned} \tag{21}$$

hold true for all $v_{1,h}, v_{2,h} \in V_h$, and for all $w_{1,h} \in W_h$. L_1, L_2 and L_3 are three positive, user-defined parameters on which only mild conditions are imposed. We refer to [36, 45, 57] for the analysis of the numerical schemes which have inspired the ones presented here. Often, one needs to properly tune these parameters to obtain a robust and relatively fast solver.

2.1.3 The nonlinear splitting approach (NonLinS). The nonlinear splitting approach for solving (9) reads:

Problem P-NonLinS: Let $j > 1$ be fixed. Let $\Psi_h^{n-1}, \Psi_h^{n,j}, c_h^{n-1}, c_h^{n,j} \in V_h$ and $\theta_h^{n-1}, \theta_h^{n,j} \in W_h$ be given, find $\Psi_h^{n,j+1} \in V_h$, and $\theta_h^{n,j+1} \in W_h$ such that

$$\begin{aligned}< \theta_h^{n,j+1} - \theta_h^{n-1}, v_{1,h} > + \\ + \Delta t < K(\theta_h^{n,j+1})(\nabla(\Psi_h^{n,j+1}) + \mathbf{e_z}), \boldsymbol{\nabla} \mathbf{v_{1,h}} > \quad = \Delta t < \mathbb{S}_1, v_{1,h} >\end{aligned} \tag{22}$$

$$\begin{aligned}\Delta t < \Psi_h^{n,j+1}, w_{1,h} >= \quad & -\Delta t < p_{cap}(\theta_h^{n,j+1}, c_h^{n,j}), w_{1,h} > + \\ & + < \tau(\theta_h^{n,j+1})(\theta_h^{n,j+1} - \theta_h^{n-1}), w_{1,h} > + \\ & + \Delta t\gamma < \Phi\left(\tfrac{\theta_h^{n,j} - \theta_h^{n-1}}{\Delta t}\right), w_{1,h} >\end{aligned} \tag{23}$$

holds true for all $v_{1,h} \in V_h$ and for all $w_{1,h} \in W_h$.

Then let $\Psi_h^{n-1}, \Psi_h^{n,j}, c_h^{n-1}, c_h^{n,j} \in V_h$ and $\theta_h^{n-1}, \theta_h^{n,j} \in W_h$ be given, $\Psi_h^{n,j+1} \in V_h$ and $\theta_h^{n,j+1} \in W_h$ are obtained from the equations above, find $c_h^{n,j+1} \in V_h$ such that

$$\begin{aligned}< \theta_h^{n,j+1}(c_h^{n,j+1} - c_h^{n-1}) + c_h^{n,j}(\theta_h^{n,j+1} - \theta_h^{n-1}), v_{2,h} > + \\ + \Delta t < D\nabla c_h^{n,j+1} + \mathbf{u}_w^{n,j+1} c_h^{n,j+1}, \nabla v_{2,h} > + \\ + \Delta t < R(c_h^{n,j+1}), v_{2,h} > \quad = \Delta t < \mathbb{S}_2, v_{2,h} >\end{aligned} \tag{24}$$

holds true for all $v_{2,h} \in V_h$. The water flux is given by $\mathbf{u_w^{n,j+1}} := -\mathbf{K}(\boldsymbol{\theta}_\mathbf{h}^{\mathbf{n,j+1}})\boldsymbol{\nabla}(\boldsymbol{\Psi}_\mathbf{h}^{\mathbf{n,j+1}} + \mathbf{e_z})$.

Observe that (22)–(23) and (24) are nonlinear. To approximate their respective solutions, one can employ, e.g., the Newton method (NonLinS-Newton) or the L-scheme (NonLinS-LS).

2.1.4 The alternate splitting Newton method (Newton-AltLinS). Applied to (9), the alternate splitting Newton method reads:

Problem P-Newton-AltLinS: Let $j > 1$ be fixed. Let $\Psi_h^{n-1}, \Psi_h^{n,j}, c_h^{n-1}$, $c_h^{n,j} \in V_h$ and $\theta_h^{n-1}, \theta_h^{n,j} \in W_h$ be given, find $\Psi_h^{n,j+1} \in V_h$, and $\theta_h^{n,j+1} \in W_h$ such that

$$\begin{aligned} &< \theta_h^{n,j+1} - \theta_h^{n-1}, v_{1,h} > + \\ &+\Delta t < K(\theta_h^{n,j})(\nabla(\Psi_h^{n,j+1}) + +\mathbf{e}_z), \nabla v_{1,h} > + \\ &+\Delta t < \partial_\theta K(\theta_h^{n,j})(\nabla(\Psi_h^{n,j}) + \mathbf{e}_z)(\theta_h^{n,j+1} - \theta_h^{n,j}), \nabla v_{1,h} > \quad = \Delta t < \mathbb{S}_1, v_{1,h} > \end{aligned} \tag{25}$$

$$\begin{aligned} \Delta t < \Psi_h^{n,j+1}, w_{1,h} >= \quad & -\Delta t < p_{cap}(\theta_h^{n,j}, c_h^{n,j}), w_{1,h} > - \\ & -\Delta t < \partial_\theta p_{cap}(\theta_h^{n,j}, c_h^{n,j})(\theta_h^{n,j+1} - \theta_h^{n,j}), w_{1,h} > + \\ & + < \tau(\theta_h^{n,j})(\theta_h^{n,j+1} - \theta_h^{n-1}), w_{1,h} > + \\ & + < \partial_\theta \tau(\theta_h^{n,j})(\theta_h^{n,j} - \theta_h^{n-1})(\theta_h^{n,j+1} - \theta_h^{n,j}), w_{1,h} > + \\ & +\Delta t \gamma < \Phi\left(\tfrac{\theta_h^{n,j} - \theta_h^{n-1}}{\Delta t}\right), w_{1,h} > \end{aligned} \tag{26}$$

hold true for all $v_{1,h} \in V_h$ and $w_{1,h} \in W_h$.

Then, with given $\Psi_h^{n-1}, \Psi_h^{n,j}, c_h^{n-1}, c_h^{n,j} \in V_h$ and $\theta_h^{n-1}, \theta_h^{n,j} \in W_h$, $\Psi_h^{n,j+1} \in V_h$ and $\theta_h^{n,j+1} \in W_h$ are obtained from the equations above, find $c_h^{n,j+1} \in V_h$ such that

$$\begin{aligned} &< \theta_h^{n,j+1}(c_h^{n,j+1} - c_h^{n-1}) + c_h^{n,j}(\theta_h^{n,j+1} - \theta_h^{n-1}), v_{2,h} > \\ &+\Delta t < D\nabla c_h^{n,j+1} + \mathbf{u}_w^{n,j+1} c_h^{n,j+1}, \nabla v_{2,h} > +\Delta t < R(c_h^{n,j}), v_{2,h} > \\ &+\Delta t < \partial_c R(c_h^{n,j})(c_h^{n,j+1} - c_h^{n,j}), v_{2,h} >= \Delta t < \mathbb{S}_2, v_{2,h} > \end{aligned} \tag{27}$$

hold true for all $v_{2,h} \in V_h$.

2.1.5 The alternate splitting L-scheme (LS-AltLinS). The alternate splitting L-scheme for solving (9) is:

Problem P-LS-AltLinS: Let $j > 1$ be fixed. Let $\Psi_h^{n-1}, \Psi_h^{n,j}, c_h^{n-1}, c_h^{n,j} \in V_h$ and $\theta_h^{n-1}, \theta_h^{n,j} \in W_h$ be given, find $\Psi_h^{n,j+1} \in V_h$, and $\theta_h^{n,j+1} \in W_h$ such that

$$\begin{aligned} &< \theta_h^{n,j+1} - \theta_h^{n-1}, v_{1,h} > + \\ &+\Delta t < K(\theta_h^{n,j})(\nabla(\Psi_h^{n,j+1}) + \mathbf{e}_z), \nabla v_{1,h} > + \\ &+L_1 < \Psi_h^{n,j+1} - \Psi_h^{n,j}, v_{1,h} >= \Delta t < \mathbb{S}_1, v_{1,h} > \end{aligned} \tag{28}$$

$$\begin{aligned}\Delta t < \Psi_h^{n,j+1}, w_{1,h} >= \; & -\Delta t < p_{cap}(\theta_h^{n,j}, c_h^{n,j}), w_{1,h} > + \\ & + < \tau(\theta_h^{n,j})(\theta_h^{n,j+1} - \theta_h^{n-1}), w_{1,h} > + \\ & + L_2 < \theta_h^{n,j+1} - \theta_h^{n,j}, w_{1,h} > + \\ & + \Delta t\gamma < \Phi\left(\frac{\theta_h^{n,j} - \theta_h^{n-1}}{\Delta t}\right), w_{1,h} >\end{aligned} \tag{29}$$

holds true for all $v_{1,h} \in V_h$ and $w_{1,h} \in W_h$.

Then, with given $\Psi_h^{n-1}, \Psi_h^{n,j}, c_h^{n-1}, c_h^{n,j} \in V_h$ and $\theta_h^{n-1}, \theta_h^{n,j} \in W_h$, and $\Psi_h^{n,j+1} \in V_h$ and $\theta_h^{n,j+1} \in W_h$ from the equations above. We find $c_h^{n,j+1} \in V_h$ such that

$$\begin{aligned} & < \theta_h^{n,j+1}(c_h^{n,j+1} - c_h^{n-1}) + c_h^{n,j}(\theta_h^{n,j+1} - \theta_h^{n-1}), v_{2,h} > \\ + \Delta t < D\nabla c_h^{n,j+1} + \mathbf{u_w^{n,j+1}} \mathbf{c_h^{n,j+1}}, \boldsymbol{\nabla} \mathbf{v_{2,h}} > + \boldsymbol{\Delta t} < \mathbf{R}(\mathbf{c_h^{n,j}}), \mathbf{v_{2,h}} > & \\ & + L_3 < c_h^{n,j+1} - c_h^{n,j}, v_{2,h} >= \Delta t < \mathbb{S}_2, v_{2,h} > \end{aligned} \tag{30}$$

hold true for all $v_{2,h} \in V_h$.

Remark 2.1. *There exist multiple improved formulations of both the Newton method and L-scheme. We refer, among others, to the trust region techniques [69], and the modified L-scheme in [49].*

Remark 2.2. *(Stopping criterion) For all schemes (monolithic or splitting), the iterations are stopped when,*

$$\|\Psi_h^{n,j+1} - \Psi_h^{n,j}\|_\infty \leq \epsilon_1, \|\theta_h^{n,j+1} - \theta_h^{n,j}\|_\infty \leq \epsilon_2 \text{ and } \|c_h^{n,j+1} - c_h^{n,j}\|_\infty \leq \epsilon_3,$$

where by $\|\cdot\|_\infty$ we mean the $L^\infty(\Omega)$ norm. Later on, for ease of presentation, we consider $\epsilon_1 = \epsilon_2 = \epsilon_3 = \epsilon$. The parameter ϵ will be defined in the numerical section.

2.2. ANDERSON ACCELERATION

Although the L-scheme is robust and converges under mild restrictions, the convergence rate depends strongly on the linearization parameters. We refer to [45, 57, 62] for the analysis in case of standard Richards equation, and to [39] for the nonstandard model. Tuning the parameters to obtain optimal results in terms of numbers of iterations and thus of computational times, can be tedious and time-consuming. The Anderson Acceleration (AA) is a powerful post-processing tool which can drastically reduce the numbers of iterations required by linearly convergent schemes, such as the L-scheme here investigated. In addiction, it reduces the need for finding close to optimal linearization parameters.

D. G. Anderson introduced the acceleration tool in 1965 [7], and since then it has been investigated in multiple works, to name a few [16, 28, 68]. We recall

here the definition of AA, presented in [68], formulated for a general fixed point problem, of the form: given $g : \mathbb{R}^n \to \mathbb{R}^n$, solve the system $x = g(x)$. Opposed to utilize only the last iteration x_k, in the AA the new approximation

Algorithm 1 Classical Fixed-Point iteration

1: Given x_0
2: **for** $k = 0, 1,...$ until convergence **do**
3: $\quad x_{k+1} = g(x_k)$
4: **end for**

is a linear combination of previously computed ones, see Algorithm 2. In the following, we denote by AA(m) the Anderson acceleration where $m + 1$ previously computed iterates are taken into account. With this, AA(0) is the non-accelerated formulation. As revealed in the test cases below, this

Algorithm 2 Anderson Acceleration AA(m)

1: Given x_0
2: **for** $k = 1, 2...$ until convergence **do**
3: $\quad$ Set $m_k = min\{m, k - 1\}$
4: $\quad$ Define the matrix $F_k = (f_{k-m_k-1}, \cdots, f_{k-1})$, where $f_i = g(x_i) - x_i$
5: $\quad$ Find $\alpha \in \mathbb{R}^{m_k+1}$ that solves

$$\min_{\alpha=(\alpha_0,\cdots,\alpha_{m_k})^T} \|\|\| F_k\alpha\| \text{s.t. } \sum_{i=0}^{m_k} \alpha_i = 1.$$

6: $\quad$ Define $x_k := \sum_{i=0}^{m_k} \alpha_i g(x_{k-m_k+i-1})$
7: **end for**

technique can drastically reduce the number of iterations required by the L-scheme.

The original formulation presented in [7] allows a for more general step,

$$x_k := \beta_k \sum_{i=0}^{m_k} \alpha_i g(x_{k-m_k+i-1}) + (1 - \beta_k) \sum_{i=0}^{m_k} \alpha_i x_{k-m_k+i-1},$$

for a user-defined tuning parameter $\beta_k \in (0, 1]$. We considered the simplified formulation, obtained with $\beta_k = 1$, because no improvements have been observed in the numerical results when using the extended one.

We remark that large values for the depth m can result in an instability of the solution algorithm. When implementing the Anderson acceleration, one has to tune this parameter properly. A small m could produce only a

small reduction in the numbers of iterations; too large m could result in a non-converging algorithm [29].

Remark 2.3. *The definition of the nonlinear splitting solvers allows for different ways to apply the AA. We study three different loops: the coupling one and the linearizing ones, one for each set of equations. We apply the Anderson acceleration to each of them. Two different parameters, m and m_{lin}, are defined. The former is used for the AA on the coupling loop, the latter for the implementation on the linearization ones. The same m_{lin} will be used for the loop regarding the flow equations and for the one regarding the transport.*

3. NUMERICAL EXAMPLES

In the following, we consider four numerical examples with increasing complexity, based on a manufactured solution, and an example in which the boundary conditions drive the flow but no manufactured solution is given. The first four will differ in the different values for γ, δ and $\tau(\theta)$ taken into account. We have implemented the models and solving schemes in MRST, a toolbox based on Matlab for the simulations of flow in porous media [44]. We use the two point flux approximation, one of the most common spatial discretization techniques. We remark that the linearization schemes and solving algorithms do not depend on the particular choice of the spatial discretization, so one may apply these solvers to other methods as well, without any difficulty.

The domain is the unit square Ω and the final time taken into consideration is $T = 3$. The simulations are performed on regular meshes, consisting of squares with sides $dx = 1/10,\ 1/20$, and $1/40$. The time steps are $\Delta t = T/25,\ T/50$ and $T/100$. The L parameters, used in the L-scheme formulations, are $L_1 = L_2 = L_3 = 0.1$, if not specified otherwise. We took into consideration different values, but the aforementioned choice seems to produce a robust algorithm which required fewest iterations to achieve the convergence. For the ease of the presentation, we set the three L parameters equal to each other; one could define different values for each parameter, investigating even further the linearization of each equation. We avoided this due to the application of the AA. We will observe that the schemes can be drastically accelerated, even though the L parameters are not optimal.

The condition numbers, for the stiffness matrices resulting from the different solving algorithms are computed using the L^1 norm, and we here report the averaged values over the full simulation. A minus sign $(-)$, in the tables reporting on iterations and condition numbers, implies that the method failed to converge for the particular combination of the time step and mesh size. The tolerance ϵ used in the stopping criterion presented in Remark 2.2 is $\epsilon = 1e-6$. We always report the total numbers of iterations required by the full simulation, not the average number required by each time step. For the

splitting solver, we present, separately, the condition numbers of both flow and transport equations. Furthermore, for the nonlinear splitting, the iterations are divided in two, the ones required by the flow equations and the ones for the transport. Finally, the condition numbers reported are obtained by averaging over the full simulations.

We apply the Anderson acceleration to each solving algorithm, always reporting the depths m and m_{lin} used. Once more, m_{lin} is the Anderson parameter used for the acceleration of the linearization loops regarding the flow and transport equations in the nonlinear splitting solvers.

Inspired by [46], the first four examples are constructed in such a way that the following is an exact solution:

$$\theta_m(x,y,t) = \begin{cases} 1 - \frac{1}{2}\cos((t_1(x,y) - t)^2) & \text{if} \quad t < t_1(x,y), \\ \frac{1}{2} & \text{if} \quad t_1(x,y) \leq t \leq t_2(x,y), \\ 1 - \frac{1}{2}\cos((t - t_2(x,y))^2) & \text{if} \quad t > t_2(x,y), \end{cases} \tag{31}$$

$$\Psi_m(x,y,t) = \begin{cases} -p_{cap}(\theta_m) + \tau(\theta_m)\partial_t\theta_m - \gamma & \text{if} \quad \partial_t\theta_m < -\delta, \\ -p_{cap}(\theta_m) + \tau(\theta_m)\partial_t\theta_m + \frac{\gamma}{\delta}\partial_t\theta_m & \text{if} \quad -\delta \leq \partial_t\theta_m \leq \delta, \\ -p_{cap}(\theta_m) + \tau(\theta_m)\partial_t\theta_m + \gamma & \text{if} \quad \partial_t\theta_m > \delta, \end{cases} \tag{32}$$

$$c_m(x,y,t) = x(x-1)y(y-1)t, \tag{33}$$

where $t_1(x,y) = xy$, $t_2(x,y) = xy + 2$. Once the manufactured water content is defined, one obtains the pressure by simply using the second equation in (5). The capillary pressure is expressed as $p_{cap}(\theta, c) = 1 - \theta^2 - 0.1\ c^3$ and the conductivity as $K(\theta) = 1 + \theta^2$. Even though such a formulation may appear non-realistic, we are mainly interested in the nonlinearities. Furthermore, a nonlinear reaction term, $R(c) = c/(c+1)$, is taken into account in the transport equation and the diffusion/dispersion coefficient D is set equal to 1.

Given the analytical expressions above, we can easily define the initial conditions, the Dirichlet boundary conditions on the unit square and compute the source terms $\mathbb{S}_1$ and $\mathbb{S}_2$ such that Ψ_m, θ_m and c_m are solutions of the system. In particular, the initial concentration and water content are

$$\begin{aligned} c(x,y,0) &= 0 && \text{on} \quad \Omega, \\ \theta(x,y,0) &= 1 - \tfrac{1}{2}\cos\left(t_1(x,y)^2\right) && \text{on} \quad \Omega. \end{aligned}$$

We impose a zero concentration $c(x,y,t) = 0$ on the boundary of the domain. The remaining boundary conditions, concerning the pressure, are time dependent. One needs to compute t_1 and t_2 on every side of the unit square. Once the time intervals given by t_1 and t_2 are obtained, the pressure can easily be

imposed. For example, on the left side $x = 0$, thus $t_1 = 0$ and $t_2 = 2$. The water content θ becomes

$$\theta(0, y, t) = \theta_{left}(t) = \begin{cases} \frac{1}{2} & \text{if} \quad 0 < t < 2, \\ 1 - \frac{1}{2}\cos((t-2)^2) & \text{if} \quad t \geq 2, \end{cases}$$

and the resulting pressure boundary condition is

$$\Psi_{left}(0, y, t) = \begin{cases} -p_{cap}(\theta_{left}) + \tau(\theta_{left})\partial_t\theta_{left} - \gamma & \text{if} \quad \partial_t\theta_{left} < -\delta, \\ -p_{cap}(\theta_{left}) + \tau(\theta_{left})\partial_t\theta_{left} + \\ +\frac{\gamma}{\delta}\partial_t\theta_{left} & \text{if} \quad -\delta \leq \partial_t\theta_{left} \leq \delta, \\ -p_{cap}(\theta_{left}) + \tau(\theta_{left})\partial_t\theta_{left} + \gamma & \text{if} \quad \partial_t\theta_{left} > \delta. \end{cases}$$

Analogously, one can compute the pressure boundary conditions on the remaining sides.

3.1. EXAMPLE 1, $\gamma = 0$, $\tau(\theta) = 1$

In the first example we impose $\gamma = 0$, thus, the hysteresis effects are neglected but we include a dynamic effect by considering a constant $\tau(\theta) = 1$. We compare the different algorithms presented in Section 2.1, reporting in the Tables 1 and 2 the total numbers of iterations required by each algorithm, and the condition numbers of the systems associated with each scheme. In the former, we investigate a fixed time step size, $\Delta t = T/25$, in the latter a fixed mesh size, $dx = 1/10$. As expected, a finer mesh results in worse conditioned systems, while smaller time steps give better conditioned ones. Moreover, the total number of iterations is increasing as we reduce the time step; smaller Δt implies more time steps and thus more iterations.

The schemes based on the L-scheme appear to be better conditioned than those based on the Newton method. The result is coherent with the theory [36, 45, 49, 57, 62]. One could even improve the condition numbers by using larger L parameters. However, larger values would have also increased the total numbers of iterations.

The alternate splitting schemes are converging much faster than the nonlinear ones. It is also interesting to observe that the numbers of iterations, required by the alternate splitting schemes, are comparable with the ones associated with the monolithic solvers. In [36], we observed similar results when solving the models without hysteresis and dynamic effects.

We notice also some reduction in the number of iterations required by the L-schemes thanks to the Anderson acceleration. The results obtained for the non-accelerated L-schemes ($m = 0$) are already optimal in terms of numbers of iterations; thus, the improvement can only be minimal. We report the total number of iterations for the full simulation, but mention that on average,

dx	Monolithic #iter.	Monolithic κ_M	NonLinS #iter.	NonLinS κ_F	NonLinS κ_T	AltLinS #iter.	AltLinS κ_F	AltLinS κ_T
	Newton		Newton			Newton		
1/10	65	4.9e+02	56 - 50	1.8e+02	1.6e+02	66	1.8e+02	1.6e+02
1/20	69	2.2e+03	57 - 50	7.6e+02	6.3e+02	66	7.6e+02	6.3+02
1/40	70	1.1e+04	58 - 50	3.2e+03	2.5e+03	66	3.4e+03	2.5e+03
	Newton(AA m = 1)		Newton (AA $m = m_{lin} = 1$)			Newton (AA m = 1)		
1/10	93	4.7e+02	65 - 50	1.8e+02	1.6e+02	74	1.8e+02	1.6e+02
1/20	98	2.1e+03	66 - 50	7.5e+02	6.3e+02	74	7.5e+02	6.3e+02
1/40	100	9.9e+03	69 - 50	3.2e+03	2.5e+03	76	3.3e+03	2.5e+03
	L-scheme		L-scheme			L-scheme		
1/10	134	4.1e+02	117 - 116	1.4e+02	1.3e+02	140	1.6e+02	1.3e+02
1/20	140	1.8e+03	119 - 115	6.9e+02	5.4e+02	144	7.3e+02	5.4e+02
1/40	146	8.5e+03	128 - 116	3.1e+03	2.1e+03	150	3.1e+03	2.1e+03
	L-scheme (AA m = 1)		L-scheme (AA $m = m_{lin} = 1$)			L-scheme (AA m = 1)		
1/10	127	4.1e+02	107 - 100	1.9e+02	1.3e+02	136	1.4e+02	1.3e+02
1/20	129	1.8e+03	111 - 100	7.9e+02	5.4e+02	142	7.1e+02	5.3e+02
1/40	130	8.8e+03	118 - 100	3.3e+03	2.1e+03	146	3.0e+03	2.0e+03

Table 1: Example 1: Total number of iterations and condition numbers for fixed $\Delta t = T/25$, and different dx. Here, $L_1 = L_2 = L_3 = 0.1$ and $m = m_{lin} = 1$.

for each time step, the L-scheme requires only five or six iterations. This is already a remarkable result, achieved thanks to the optimal L parameters. Furthermore, the Newton solvers have resulted in being slower when combined with the AA. This is coherent with the theory where it has been observed that quadratically convergent schemes, cannot be improved and the resulting accelerated solvers appear slower [28].

In Table 3 we present the numerical errors and the estimated order of convergence of the spatial discretization based on the successively refined meshes investigated. Given the manufactured solution Ψ_m, we compute the numerical error $e_\Psi = |||| \Psi_m - \Psi_n ||||$, where Ψ_n is the numerical pressure computed. Similarly, we can define e_θ and e_c. Furthermore, $e_{\Psi,1}$ is the numerical error obtained for the mesh size $dx = 1/10$ and $\Delta t = T/25$, $e_{\Psi,2}$ for $dx = 1/20$ and $\Delta t = T/50$, and finally $e_{\Psi,3}$ for $dx = 1/40$ and $\Delta t = T/100$. $EOC = \log\left(\frac{e_{\Psi,i}}{e_{\Psi,i+1}}\right) / \log(2)$ is the estimated order of convergence. These results are independent from the solving algorithm taken into account, only the discretization approach plays a role. In this case we use a TPFA which is known to have a order of convergence equal to 1, as also reported here in the table.

Δt	Monolithic #iter.	Monolithic κ_M	NonLinS #iter.	NonLinS κ_F	NonLinS κ_T	AltLinS #iter.	AltLinS κ_F	AltLinS κ_T
	Newton		Newton			Newton		
T/25	65	4.9e+02	56 - 50	1.8e+02	1.6e+02	66	1.8e+02	1.6e+02
T/50	103	2.7e+02	98 - 50	1.2e+02	8.8e+01	99	1.2e+02	8.8e+01
T/100	186	1.9e+02	172 - 50	8.6e+01	4.7e+01	172	8.7e+01	4.7e+01
	Newton(AA m = 1)		Newton (AA $m = m_{lin} = 1$)			Newton (AA m = 1)		
T/25	93	4.7e+02	65 - 50	1.8e+02	1.6e+02	74	1.8e+02	1.6e+02
T/50	137	2.7e+02	114 - 50	1.2e+02	8.8e+01	114	1.2e+02	8.8e+01
T/100	244	1.9e+02	201 - 100	8.5e+01	4.7e+01	200	8.6e+01	4.7e+01
	L-scheme		L-scheme			L-scheme		
T/25	134	4.1e+02	117 - 116	1.4e+02	1.3e+02	140	1.6e+02	1.3e+02
T/50	219	2.3e+02	182 - 200	1.1e+02	7.5e+01	218	1.2e+02	7.5e+01
T/100	425	1.6e+02	346 - 400	8.3e+01	3.9e+01	438	8.2e+01	3.9e+01
	L-scheme (AA m = 1)		L-scheme (AA $m = m_{lin} = 1$)			L-scheme (AA m = 1)		
T/25	127	4.1e+02	107 - 100	1.9e+02	1.3e+02	136	1.4e+02	1.3e+02
T/50	217	2.3e+02	192 - 160	1.2e+02	7.5e+01	238	1.1e+02	7.5e+01
T/100	387	1.6e+02	347 - 300	8.3e+01	3.9e+01	432	8.2e+01	3.9e+01

Table 2: Example 1: Total number of iterations and condition numbers for fixed $dx = 1/10$, and different Δt. Here $L_1 = L_2 = L_3 = 0.1$, $m = m_{lin} = 1$.

	e_1	EOC	e_2	EOC	e_3
Ψ	4.61e-02	0.98	2.33e-02	1.00	1.16e-02
θ	1.31e-02	0.97	6.71e-03	0.99	3.38e-03
c	6.24e-03	1.53	2.15e-03	1.32	8.60e-04

Table 3: Example 1: Numerical error and estimated order of convergence (EOC) of the discretization method.

In Table 4 we tested different values of m and L. We can observe that, for large L, the Monolithic L-Scheme, here investigated, requires more iterations than for smaller parameters. If many iterations are required to achieve the convergence at each time step, one can take in consideration larger m values. For $L = 0.1$, the optimal choice, in terms of numbers of iterations, is $m = 1$; larger values result in slightly slower schemes. For the largest L tested, $L = 2.3$, the optimal choice is $m = 2$. Such L value corresponds to the theoretical L, $\max_\theta\{\frac{\partial p_{cap}}{\partial \theta}\} \approx 2.3$. To ensure the monotone convergence of the scheme it has been proved, that the parameter chosen must be larger than the Lipschitz

constant of the nonlinearity, in this case the capillary pressure as a function of θ (see [45, 57, 62]). We set L_1, L_2 and L_3 equal to the theoretical L computed for the capillary pressure.

We can conclude that it is possible to obtain significant improvements by investigating the AA and thus finding the appropriate depth m. In this work, we have focused more on individuating the optimal L parameters, as refining the AA can be done more easily. The depths used are, in fact, small natural numbers.

L	$m=0$	$m=1$	$m=2$	$m=3$	$m=5$
.1	146	130	146	179	215
.5	247	161	152	172	200
1	411	202	168	165	195
2	711	290	199	206	217
2.3	810	317	207	215	227

Table 4: Example 1: Comparison of number of iterations for different m and L parameters for L-Mono.
Here, $dx = 1/40$, $\Delta t = T/25$ and $L_1 = L_2 = L_3 = L$.

Finally, we investigate the order of convergence of the linearization schemes. In Figure 5, we plot the residuals of pressure, water content and concentration, obtained at the final time step for the finest mesh size, $dx = 1/40$ and $\Delta t = T/25$. We can deduce the rates of convergence of the different linearization schemes. The L-schemes appear to be, as expected, linearly convergent in term of numbers of iterations. The AA improves the results only slightly, as already observed in Tables 1 and 2. This is justified by the fact that the L parameters (L_1, L_2, L_3) chosen here, appear to be optimal. The Newton methods are instead quadratically convergent. More precise results are observable in Table 5. Here we present the exact order of convergence of the different schemes. Given the residual of each unknown $(res_\Psi, res_\theta, res_c)$, at each iteration j, we compute the order of convergence as follow: $ORD_j = \big(\log(res_{j+1}/res_j)\big)/\big(\log(res_j/res_{j-1})\big)$. For a fixed time step, we can average the orders obtained over the number of iterations required to achieve the convergence. We report below the values obtained by investigating the final time step; similar results have been observed for previous time steps.

Remark 3.1. *Since the Anderson acceleration with small depth is a cheap post-processing step, reducing the number of iterations directly reduces the CPU time almost proportionally.*

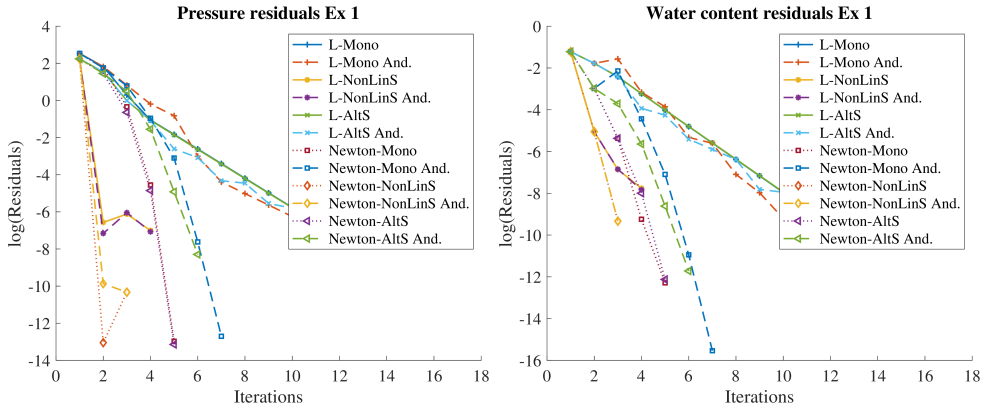

(a) Pressure residuals.

(b) Water content residuals.

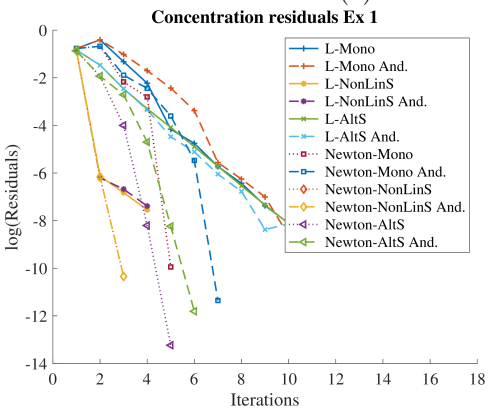

(c) Concentration residuals.

Fig. 5.: Example 1: Residuals of each unknown at the final time step, for the different schemes. Here, $L_1 = L_2 = L_3 = 0.1$, $m = m_{lin} = 1$, $dx = 1/40$, $\Delta t = T/25$.

3.2. EXAMPLE 2, $\gamma = 0$, $\tau(\theta) = 1 + \theta^2$

In the second example, the setup of the first is extended by adopting a nonlinear τ, precisely $\tau(\theta) = 1 + \theta^2$. In Tables 6 and 7, we present the condition numbers and the required iteration counts associated with each solving algorithm.

The introduction of a nonlinear $\tau(\theta)$ increases the numbers of iterations required by each solver. The L-scheme is linearly convergent while the Newton method is quadratically convergent. Furthermore, the conclusions from Example 1 concerning the AA remain the same. In particular, we observe

	Ls Mono	Ls NonLinS And.	Ls NonLinS	Ls NonLinS And.	Ls AltLinS	Ls AltLinS And.
Ψ	1.00	1.26	1.13	1.46	1.13	2.07
c	0.96	1.55	1.01	1.77	1.01	1.30
θ	1.01	1.40	0.89	1.01	0.94	1.32
	New. Mono	New. NonLinS And.	New. NonLinS	New. NonLinS And.	New. AltLinS	New. AltLinS And.
Ψ	2.03	1.61	1.94	1.86	2.04	2.03
c	2.41	2.01	1.61	1.41	1.85	1.46
θ	1.97	0.57	1.81	0.97	1.61	0.95

Table 5: Example 1: Estimated order of convergence for the different linearization schemes.

	Monolithic		NonLinS			AltLinS		
dx	#iter.	κ_{M}	#iter.	κ_{F}	κ_{T}	#iter.	κ_{F}	κ_{T}
	Newton		Newton			Newton		
1/10	67	481.17	59 - 50	161.39	161.00	64	152.62	161.76
1/20	69	2.2e+03	57 - 50	656.26	636.33	66	644.98	644.99
1/40	70	1.1e+04	59 - 50	2.8e+03	2.5e+03	68	2.9e+03	2.5e+03
	Newton(AA m = 1)		Newton (AA $m = m_{lin} = 1$)			Newton (AA m = 1)		
1/10	94	467.04	69 - 50	160.36	161.00	76	152.45	161.94
1/20	98	2.1e+03	68 - 50	636.14	636.33	76	642.25	638.40
1/40	100	9.8e+03	71 - 50	2.8e+03	2.5e+03	80	2.9e+03	2.5e+03
	L-scheme		L-scheme			L-scheme		
1/10	136	403.49	112 - 117	158.33	137.81	130	158.05	138.50
1/20	139	1.7e+03	120 - 116	644.85	544.34	136	651.07	545.85
1/40	144	8.3e+03	125 - 116	2.7e+03	2.1e+03	142	2.8e+03	2.1e+03
	L-scheme (AA m = 1)		L-scheme (AA $m = m_{lin} = 1$)			L-scheme (AA m = 1)		
1/10	129	401.61	106 - 100	158.87	137.74	132	156.89	138.21
1/20	131	1.7e+03	113 - 100	644.63	543.86	134	647.35	545.18
1/40	137	8.4e+03	117 - 100	2.7e+03	2.1e+03	142	2.7e+03	2.1e+03

Table 6: Example 2: Total number of iterations and condition numbers for fixed $\Delta t = T/25$, and different dx. Here, $L_1 = L_2 = L_3 = 0.1$ and $m = m_{lin} = 1$.

only small reductions in the numbers of iterations required by the L-schemes. Once more, this is justified by the optimal choice of the L parameters. We can observe that, for each time step, only a few iterations are required; thus, no further acceleration is expected.

Δt	Monolithic #iter.	Monolithic κ_M	NonLinS #iter.	NonLinS κ_F	NonLinS κ_T	AltLinS #iter.	AltLinS κ_F	AltLinS κ_T
	Newton		Newton			Newton		
T/25	67	481.17	59 - 50	161.39	161.00	64	152.62	161.76
T/50	107	256.90	102 - 50	95.40	89.26	102	95.08	89.80
T/100	193	159.33	184 - 100	73.42	47.70	184	72.37	47.91
	Newton(AA m = 1)		Newton (AA $m = m_{lin} = 1$)			Newton (AA m = 1)		
T/25	94	467.04	69 - 50	160.36	161.00	76	152.45	161.94
T/50	142	254.28	117 - 50	94.64	89.26	118	95.71	89.88
T/100	259	159.96	207 - 100	73.05	47.70	208	72.78	47.95
	L-scheme		L-scheme			L-scheme		
T/25	136	403.49	112 - 117	157.86	137.81	130	158.05	138.50
T/50	220	211.60	185 - 201	98.63	75.62	220	97.80	75.86
T/100	433	125.49	356 - 400	65.18	40.16	446	65.24	40.28
	L-scheme (AA m = 1)		L-scheme (AA $m = m_{lin} = 1$)			L-scheme (AA m = 1)		
T/25	129	401.61	106 - 100	158.87	137.74	132	156.89	138.21
T/50	214	212.13	192 - 161	97.72	75.69	240	97.63	75.66
T/100	388	126.15	355 - 302	64.73	40.16	440	64.45	40.17

Table 7: Example 2: Total number of iterations and condition numbers for fixed $dx = 1/10$, and different Δt. Here $L_1 = L_2 = L_3 = 0.1$, $m = m_{lin} = 1$.

As for the results presented in Tables 6 and 7, the numerical errors and EOC reported in Table 8 are similar to the ones from the first example.

	e_1	EOC	e_2	EOC	e_3
Ψ	0.0759	0.9688	0.0388	0.9913	0.0195
θ	0.0140	0.9556	0.0072	0.9830	0.0036
c	0.0084	1.5198	0.0029	1.3037	0.0012

Table 8: Example 2: Numerical error and estimated order of convergence (EOC) of the discretization method.

In Figure 6, we report the residuals of the pressure, water content and concentration at the final time step. The L-schemes are linearly convergent, and applying the AA does not result in significant improvements. The convergence rates and number of iterations remain the same. Also for the Newton solvers, since they are quadratically convergent, the AA cannot improve this aspect. Table 9 presents the precise order of convergence of the different linearization schemes.

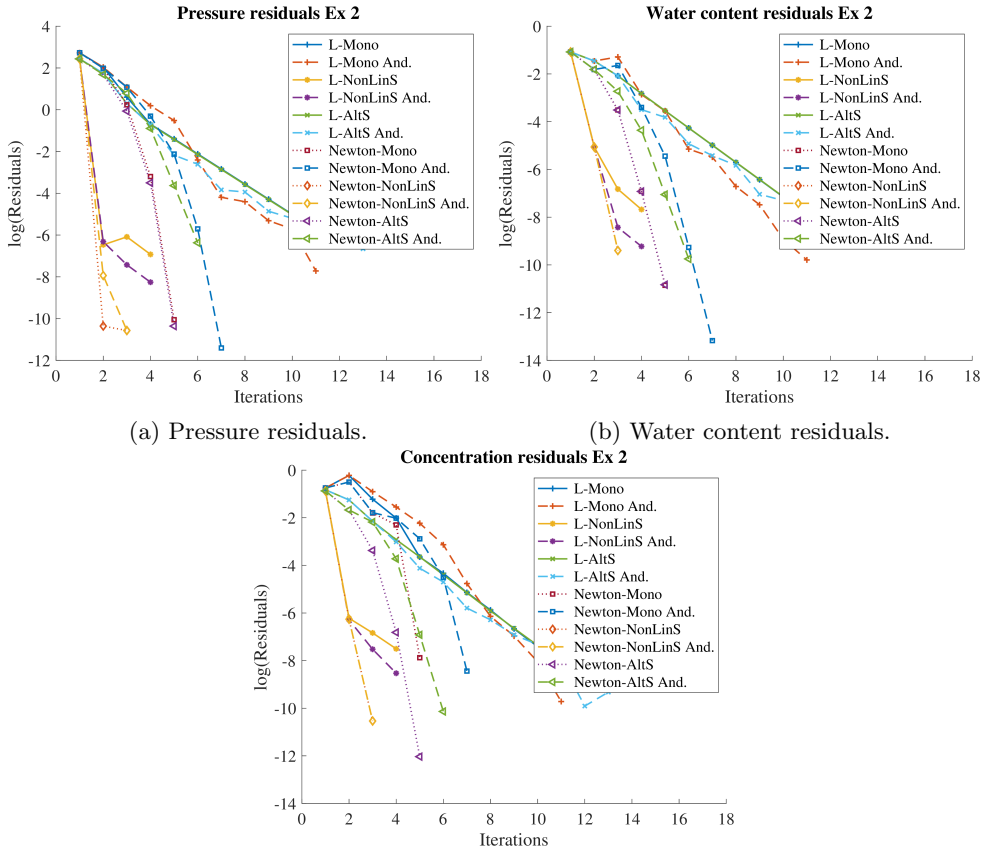

(a) Pressure residuals.

(b) Water content residuals.

(c) Concentration residuals.

Fig. 6.: Example 2: Residuals of each unknown at the final time step, for the different schemes. Here, $L_1 = L_2 = L_3 = 0.1$, $m = m_{lin} = 1$, $dx = 1/40$, $\Delta t = T/25$.

3.3. EXAMPLE 3, $\gamma = 1$, $\delta = 5E - 3$, $\tau(\theta) = 0$

With the same manufactured solutions, we now consider the case without dynamic effects ($\tau(\theta) = 0$), but include hysteresis by choosing $\gamma = 1$ and $\delta = 5e - 3$.

From the results in Tables 10 and 11, we notice that the Newton method, in all its formulations, fails to converge. In Table 11, smaller time steps are taken, but no improvements are observable. A further reduction of the time step could have resulted in converging Newton solvers but the total numbers of iterations for the full simulation would have been larger than the ones required

	Ls Mono	Ls NonLinS And.	Ls NonLinS	Ls NonLinS And.	Ls AltLinS	Ls AltLinS And.
Ψ	1.07	1.40	1.11	1.36	1.14	1.24
c	0.99	1.23	0.98	1.45	0.96	1.10
θ	1.03	1.15	0.97	1.25	0.93	0.98
	New. Mono	New. NonLinS And.	New. NonLinS	New. NonLinS And.	New. AltLinS	New. AltLinS And.
Ψ	1.61	1.58	1.97	1.69	2.15	2.14
c	2.68	1.47	1.98	1.54	1.98	1.83
θ	1.99	1.61	1.89	1.70	2.17	1.95

Table 9: Example 2: Estimated order of convergence for the different linearization schemes.

by the L-schemes on fewer but larger time steps. In contrast, the L-schemes are more robust and, even though requiring a higher number of iterations than previously, they converge. We take $L_1 = L_2 = L_3 = L = 1$, which appear to be the optimal choice in terms of numbers of iterations.

The AA improves the convergence of the L-schemes. This is the first example of this study in which the results obtained thanks to the AA are improved substantially. This is due to the presence of the hysteresis, requiring a large L for the overall convergence, and thus the total numbers of iterations is larger. On average, the monolithic L-scheme solver requires circa 18 iterations per time step. For $m = 1$, the AA reduces the iterations by circa 50%. Different m values have been tested but none of the ones investigated lead to the convergence of the Newton schemes. On all tests, Newton has failed to converge, whereas the L-schemes converged and the AA yields further improvement.

dx	Monolithic #iter.	Monolithic κ_M	NonLinS #iter.	NonLinS κ_F	NonLinS κ_T	AltLinS #iter.	AltLinS κ_F	AltLinS κ_T
	Newton		Newton			Newton		
1/10	-	-	-	-	-	-	-	-
1/20	-	-	-	-	-	-	-	-
1/40	-	-	-	-	-	-	-	-
	L-scheme		L-scheme			L-scheme		
1/10	448	409.16	210 - 441	484.83	69.22	450	361.76	69.34
1/20	456	1.6e+03	266 - 439	1.9e+03	259.35	452	1.4e+03	260.02
1/40	468	6.6e+03	276 - 438	7.7e+03	996.36	460	5.8e+03	999.13
	L-scheme (AA m = 2)		L-scheme (AA m=2 $m_{lin} = 5$)			L-scheme (AA m = 1)		
1/10	226	468.28	179 - 150	497.56	70.10	328	450.28	71.81
1/20	278	1.9e+03	187 - 141	2.0e+03	261.40	408	2.0e+03	269.72
1/40	303	8.2e+03	-	-	-	378	7.7e+03	967.29

Table 10: Example 3: Total number of iterations and condition numbers for fixed $\Delta t = T/25$, and different dx. Here, $L_1 = L_2 = L_3 = 1$, different m and m_{lin} are taken into account.

Δt	Monolithic #iter.	Monolithic κ_M	NonLinS #iter.	NonLinS κ_F	NonLinS κ_T	AltLinS #iter.	AltLinS κ_F	AltLinS κ_T
	Newton		Newton			Newton		
T/25	-	-	-	-	-	-	-	-
T/50	-	-	-	-	-	-	-	-
T/100	-	-	-	-	-	-	-	-
	L-scheme		L-scheme			L-scheme		
T/25	448	409.16	210 - 441	484.83	69.22	450	361.76	69.34
T/50	836	363.15	513 - 846	422.16	35.96	838	332.02	36.03
T/100	1787	395.55	1261 - 1597	428.24	18.91	1764	363.40	19.07
	L-scheme (AA m = 1)		L-scheme (AA m=2 $m_{lin} = 5$)			L-scheme (AA m = 1)		
T/25	226	468.28	179 - 150	497.56	70.10	328	450.28	71.81
T/50	533	410.93	346 - 316	504.00	36.85	664	442.54	37.43
T/100	1217	467.07	861 - 944 ($m_{lin} = 1$)	491.24	19.15	1842	473.32	19.75

Table 11: Example 3: Total number of iterations and condition numbers for fixed $dx = 1/10$, and different Δt. Here, $L_1 = L_2 = L_3 = 1$, different m and m_{lin} are taken into account

Once more, we report the numerical errors and the estimated orders of convergence associated with the discretization technique here implemented

(TPFA). In Table 12, we present the values obtained for the monolithic L-scheme. The EOC depends only on the discretization technique, not the linearization scheme or solving algorithm.

	e_1	EOC	e_2	EOC	e_3
Ψ	0.0308	1.0345	0.0150	0.9281	0.0085
θ	0.0350	1.2985	0.0142	1.0997	0.0066
c	0.0060	1.3202	0.0024	1.3000	0.0010

Table 12: Example 3: Numerical error and estimated order of convergence (EOC) of the discretization method.

In Figure 7, we report the residuals of pressure, water content and concentration, at the final time step. The differences between the accelerated and non-accelerated schemes seem to be minimal at the final time step but we observe in Tables 10 and 11 that the total improvements are actually substantial. The precise orders of convergence for the different solving algorithms are reported in Table 13. The non-accelerated L-schemes have an order of convergence equal to one, while the accelerated ones have slightly larger values. No result was reported for the Newton schemes due to the lack of convergence.

	Ls Mono	Ls NonLinS And.	Ls NonLinS	Ls NonLinS And.	Ls AltLinS	Ls AltLinS And.
Ψ	1.14	1.33	1.00	1.19	1.00	1.81
c	1.00	1.32	1.00	1.51	0.99	1.52
θ	1.00	1.29	1.00	1.39	1.00	1.16

Table 13: Example 3: Estimated order of convergence for the different linearization schemes.

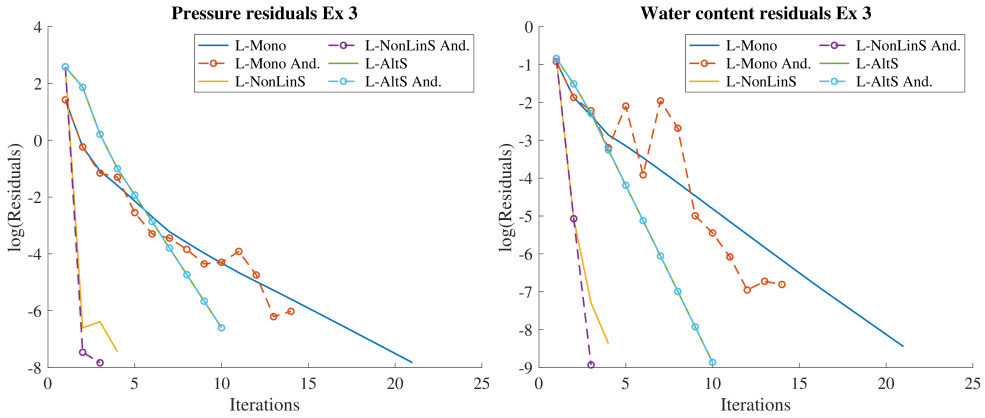

(a) Pressure residuals. (b) Water content residuals.

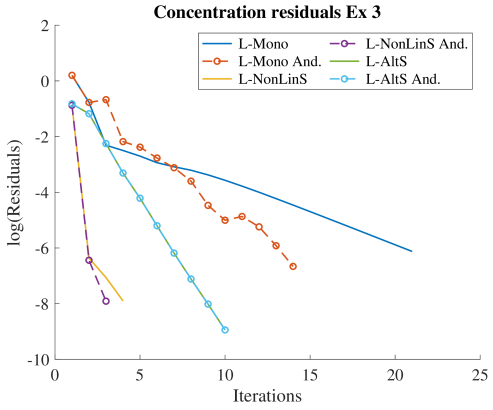

(c) Concentration residuals.

Fig. 7.: Example 3: residuals of each unknown at the final time step, for the different schemes. Here, $L_1 = L_2 = L_3 = 1$, $dx = 1/40$, $\Delta t = T/25$ and $m \neq m_{lin}$.

3.4. EXAMPLE 4, $\gamma = 1$, $\delta = 5E - 3$, $\tau(\theta) = 1 + \theta^2$

Finally, we study a problem which includes both hysteresis and dynamic capillary effects. We choose $\delta = 5e - 3$, $\gamma = 1$ and $\tau(\theta) = 1 + \theta^2$. As for the previous examples, we report the total numbers of iterations required by each algorithm, the condition numbers associated with the linearized equations, the EOC of the discretization technique and the residual for each unknown.

In Tables 14 and 15, we present the total number of iterations required by each algorithm, and the condition numbers associated with each system.

As in the previous example, the Newton method fails to converge, while the L-scheme based solvers present no difficulties. The L parameters are all set equal to 0.1. This leads to a faster convergence, when compared to the previous example, where larger values have been required for robustness. This is explained by the fact that, since the dynamic effects are introduced ($\tau > 0$), the solution is more regular [19, 47].

We have tested different values of m on the Newton methods, but none ensured the convergence of the schemes. As in the previous test cases, we have investigated smaller time steps, but the Newton solvers has still failed to converge.

Regarding the results obtained thanks to the AA, we can notice some improvements which are smaller than the ones observed for the previous test cases. Once more, this is due to the optimal choice of the L parameters, ensuring that the L-scheme converges, on average, in 5 iterations per time step. Therefore further improvements are not expected. Note that, compared to the first example (Table 4), larger L values are used leading to larger numbers of iterations. This explains why the AA with proper parameters m have improved the convergence behaviour of the L-scheme there.

	Monolithic		NonLinS			AltLinS		
dx	#iter.	κ_{M}	#iter.	κ_{F}	κ_{T}	#iter.	κ_{F}	κ_{T}
	Newton		Newton			Newton		
1/10	-	-	-	-	-	-	-	-
1/20	-	-	-	-	-	-	-	-
1/40	-	-	-	-	-	-	-	-
	L-scheme		L-scheme			L-scheme		
1/10	152	290.13	128 - 122	208.09	162.46	251	206.24	174.77
1/20	160	768.54	137 - 121	558.01	621.77	259	486.23	598.01
1/40	165	3.0e+03	141 - 120	2.1e+03	2.3e+03	328	2.1e+03	2.4e+03
	L-scheme (AA m = 1)		L-scheme (AA m=2 $m_{lin} = 3$)			L-scheme (AA m = 3)		
1/10	139	288.40	112 - 85	212.29	165.24	152	198.15	166.47
1/20	144	752.41	117 - 89	550.05	630.43	162	522.01	636.00
1/40	149	3.0e+03	127 - 88	2.1e+03	2.3e+03	166	2.0e+03	2.4e+03

Table 14: Example 4: Total number of iterations and condition numbers for fixed $\Delta t = T/25$, and different dx. Here, $L_1 = L_2 = L_3 = 0.1$ and $m \neq m_{lin}$.

Δt	Monolithic #iter.	Monolithic κ_M	NonLinS #iter.	NonLinS κ_F	NonLinS κ_T	AltLinS #iter.	AltLinS κ_F	AltLinS κ_T
	Newton		Newton			Newton		
T/25	-	-	-	-	-	-	-	-
T/50	-	-	-	-	-	-	-	-
T/100	-	-	-	-	-	-	-	-
	L-scheme		L-scheme			L-scheme		
T/25	152	290.13	128 - 122	208.09	162.46	251	206.24	174.77
T/50	248	310.93	201 - 225	264.09	89.64	424	263.91	97.09
T/100	508	415.80	403- 405	403.31	47.53	768	403.81	52.72
	L-scheme (AA m = 1)		L-scheme (AA m=2 $m_{lin} = 3$)			L-scheme (AA m = 2)		
T/25	139	288.40	112 - 85	212.29	165.24	152	198.15	166.47
T/50	233	312.95	195 - 167	267.27	90.55	250	260.41	91.42
T/100	448	416.05	358 - 308	404.34	47.65	506	403.30	48.38

Table 15: Example 4: Total number of iterations and condition numbers for fixed $dx = 1/10$, and different Δt. Here $L_1 = L_2 = L_3 = 0.1$ and $m \neq m_{lin}$

The numerical errors and the estimated orders of convergence of the discretization technique (TPFA), presented in Table 16, are consistent with the ones from the previous test cases.

	e_1	EOC	e_2	EOC	e_3
Ψ	0.0759	0.9558	0.0391	0.8837	0.0212
θ	0.0138	0.9115	0.0073	0.9463	0.0038
c	0.0101	1.2531	0.0042	1.2655	0.0018

Table 16: Example 4: Numerical error and estimated order of convergence (EOC) of the discretization method.

Finally, regarding the order of convergence of the different solving algorithms, Figure 8 presents the residuals for each unknown, and Table 17 the precise orders computed averaging over iterations at the final time step.

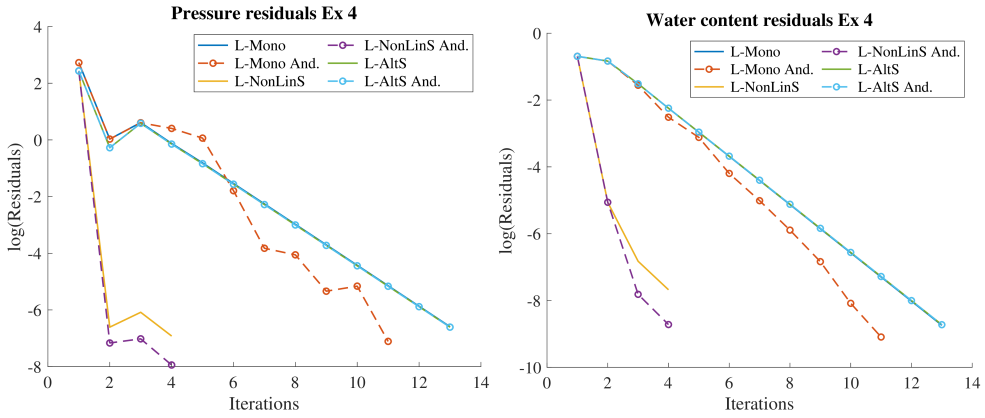

(a) Pressure residuals. (b) Water content residuals.

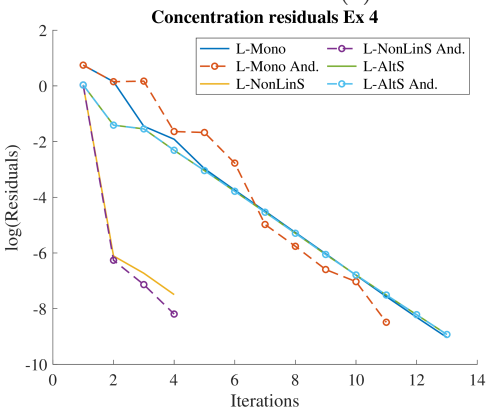

(c) Concentration residuals.

Fig. 8.: Example 4: Residuals of each unknown at the final time step, for the different schemes. Here, $L_1 = L_2 = L_3 = 0.1$, $dx = 1/40$, $\Delta t = T/25$ and different $m \neq m_{lin}$.

3.5. PHYSICAL EXAMPLE

As final numerical study, we investigate a test case that involves realistic parameters, but without having a manufactured solution. The flow will be driven by the boundary conditions. The domain Ω is the vertical column $[0,1]\times[0,2]$ and the final time is $T = 4$. This can represent a vertical section of the subsurface on which infiltration and drying processes can take place. The capillary pressure and conductivity expressions are given by the van Genuchten formulation [31], $K(\theta) = \theta_e^l\left(1-\left(1-\theta_e^{1/M}\right)^M\right)^2$ and $p_{cap}(\theta, c) = \left(1-b\ln(c/a+\right.$

	Ls Mono	Ls NonLinS And.	Ls NonLinS	Ls NonLinS And.	Ls AltLinS	Ls AltLinS And.
Ψ	1.00	1.29	0.99	1.27	0.99	1.30
c	1.29	1.29	1.02	1.15	1.07	1.11
θ	1.00	1.16	1.00	1.35	1.00	1.20

Table 17: Example 4: Estimated order of convergence for the different linearization schemes.

$1)\big)^{-1}(-\theta^{-1/M})^{1-M}$,
where $\theta_e = (\theta-\theta_r)/(\theta_s-\theta_r)$ is the effective water content, $\theta_s = 0.9$, $\theta_r = 0.005$, $M = 2$, $l = 0.31$, $a = 0.04$ and $b = 0.47$. Furthermore, we take $\tau(\theta) = 1 + \theta^2$, and the hysteresis effects are included by setting $\gamma = 1$ and $\delta = 5e-3$, as in Example 4.

Dirichlet boundary conditions are imposed at the top side of the column

$$\Psi|_{y=2} = 1 + \begin{cases} 0.5t & \text{if } t < 1, \\ 0.5 & \text{if } 1 \le t < 2, \\ 0.5(3-t) & \text{if } 2 \le t < 3, \\ -0.4 & \text{if } 3 \le t \le 4, \end{cases}$$

$$c|_{y=2} = 2,$$

whereas, at the remaining sides, we consider homogeneous Neumann boundary conditions. The discontinuity in time $t = 3$ makes solving the problem numerically even more complex. The initial conditions are

$$\theta^0 = x, \qquad \text{and} \qquad c^0 = 1.$$

The L parameters, if not otherwise specified, are set to $L = 2$. We have tested different values, but, $L = 2$ seems to give the best results in terms of numbers of iterations. Furthermore, the results may be improved even further by choosing different values for each parameter, L_1, L_2 and L_3, but for ease of presentation this has been omitted here.

In Tables 18 and 19, we report the total numbers of iterations and condition numbers associated to each algorithm. We observe that, due to the higher nonlinearities of the conductivity K and capillary pressure p_{cap} involved, the results are different compared to the ones presented for the previous examples.

Again, the Newton solvers have failed to converge and the systems associated with the linearized equations are badly conditioned. Considering smaller time steps did not resolve this.

The L-schemes on the other hand converge, but require high numbers of iterations. In case of finer meshes, one may need to use a larger L parameter.

Once more, we can observe significant improvement thanks to the AA. The performance of the monolithic solver is for example considerably improved. Furthermore, the AA can also introduce some instabilities, and thus a larger L may again be required. Clearly, this leads to an increase in the number of iterations. Such results are still better than the one obtained for smaller L with no acceleration. Similar observations can also be made for the splitting solvers. Even though larger L parameters may be necessary, the accelerated schemes perform better then the non-accelerated ones. The nonlinear splitting seems to be less stable than the alternate linear one. It also requires more iterations, and thus the alternate solver here proposed appears once more to be the better alternative. We can observe as for the finest mesh, an optimal m was not found for the AA and the schemes could not be further improved.

Moreover, it is interesting to observe the results reported in Table 19, there, the mesh size is fixed while the time step is reduced. As previously stated, the time reduction did not improve the Newton solvers, which failed to converge for all the meshes and Δt tested. Furthermore, smaller time steps can result in L-scheme solvers having worse rate of convergence. We can observe as, e.g., no results are reported for the monolithic L-scheme in case of $\Delta t = T/50$ and $\Delta t = T/100$. In these cases, the solver was stopped because the number of iterations required to achieve the convergence has exceed the value of 1000 iterations per time step.

	Monolithic		NonLinS			AltLinS		
dx	#iter.	κ_{M}	#iter.	κ_{F}	κ_{T}	#iter.	κ_{F}	κ_{T}
	Newton		Newton			Newton		
1/10	-	-	-	-	-	-	-	-
1/20	-	-	-	-	-	-	-	-
1/40	-	-	-	-	-	-	-	-
	L-scheme		L-scheme			L-scheme		
1/10	5398	612.92	6472 - 727	402.04	58.15	6772	310.28	58.15
1/20	5379	2.6e+03	8336 - 910 ($L = 2.5$)	1.6e+03	188.54	6922	1.6e+03	228.85
1/40	10281 ($L = 4$)	2.1e+03	16441 - 1751 ($L = 5$)	5.1e+03	396.37	6846	7.5e+03	911.66
	L-scheme (AA m = 1)		L-scheme (AA m=m_{lin} = 1)			L-scheme (AA m = 1)		
1/10	1454 ($L = 4$)	564.05	4572 - 542 ($L = 5$)	223.15	28.35	2480 ($L = 5$)	185.00	25.84
1/20	2333 ($L = 8$)	1.8e+03	8756 - 942 ($L = 10$)	542.12	60.21	4379 ($L = 10$)	469.75	51.59
1/40	-	-	-	-	-	-	-	-

Table 18: Example 5: Total number of iterations and condition numbers for fixed $\Delta t = T/25$, and different dx. Here, $L_1 = L_2 = L_3 = 2$ and $m \neq m_{lin}$.

Δt	Monolithic #iter.	Monolithic κ_M	NonLinS #iter.	NonLinS κ_F	NonLinS κ_T	AltLinS #iter.	AltLinS κ_F	AltLinS κ_T
	Newton		Newton			Newton		
T/25	-	-	-	-	-	-	-	-
T/50	-	-	-	-	-	-	-	-
T/100	-	-	-	-	-	-	-	-
	L-scheme		L-scheme			L-scheme		
T/25	5398	612.92	6472 - 727	402.04	58.15	6772	310.28	58.15
T/50	-	-	23033 - 1423	386.31	30.49	23994	297.65	30.50
T/100	-	-	82500 - 2886	377.15	16.22	-	-	-
	L-scheme (AA m = 1)		L-scheme (AA m=m_{lin} = 1)			L-scheme (AA m = 1)		
T/25	1454 ($L = 4$)	564.05	4572 - 542 ($L = 5$)	223.15	28.35	2480 ($L = 5$)	185.00	25.84
T/50	-	-	-	-	-	9474 ($L = 6$)	147.99	11.56
T/100	-	-	-	-	-	43488 ($L = 10$)	115.05	4.24

Table 19: Example 5: Total number of iterations and condition numbers for fixed $dx = 1/20$, and different Δt. Here, $L_1 = L_2 = L_3 = 2$ and $m \neq m_{lin}$.

In Table 20, we report the different m and m_{lin} values investigated for the AA. We observe that for the L-scheme Mono solver, the optimal choice, in terms of numbers of iterations is $m = 1$. Larger depths m may require large L parameters and thus larger numbers of iterations. For the nonlinear splitting solver, only one value of m_{lin} has been taken in consideration for the coupling loop, precisely $m_{lin} = 1$. This is justified by the fact that the majority of the iterations have taken place in the inside loops, the nonlinearities of the equations are playing a larger role than the coupling aspect.

	# it. m=0	# it. m=1	# it. m=2	# it. m=5
Mono L-scheme	5398	1454	2307 ($L = 10$)	3511 ($L = 12$)
NonLinS L-scheme	6472 - 727	4572 - 542 ($L = 5$)	-	-
AltLinS L-scheme	6772	2480 ($L = 5$)	2479 ($L = 5$)	5023 ($L = 12$)
Newton-Mono	-	-	-	-

Table 20: Example 5: Numbers of iterations associated to different m and m_{lin} values, $dx = 1/10$ $dt = T/25$.

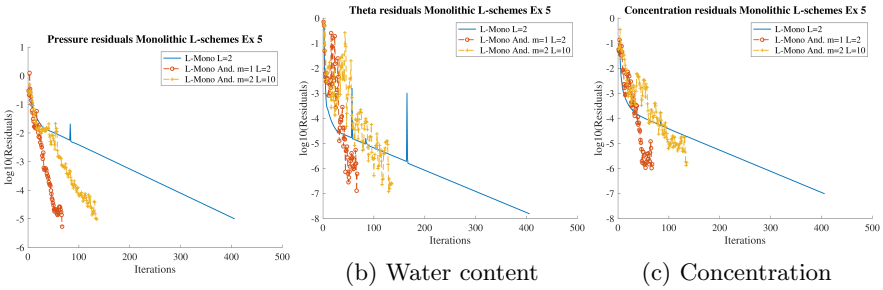

(a) Pressure residuals. (b) Water content residuals. (c) Concentration residuals.

Fig. 9.: Example 5: Residuals of each unknown at the final time step, monolithic L-scheme. Here, different L and m are tested, $dx = 1/10$, and $\Delta t = T/25$.

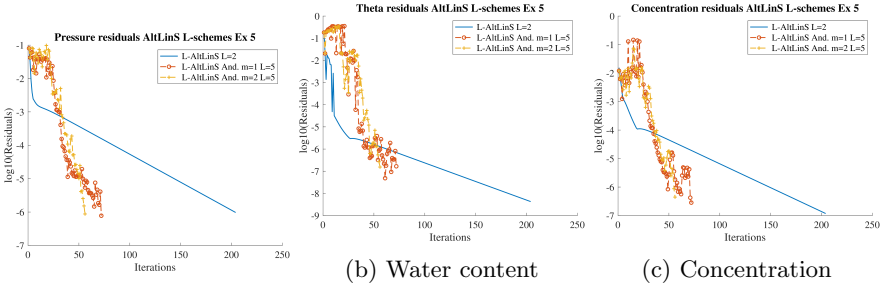

(a) Pressure residuals. (b) Water content residuals. (c) Concentration residuals.

Fig. 10.: Example 5: Residuals of each unknown at the final time step, AltLinS L-scheme. Here, different L and m are tested, $m_{lin} = 1$, $dx = 1/10$, and $\Delta t = T/25$.

Finally, in the Figures 9, 10 and 11 we report the residuals at the final time step, for each unknown and each algorithm, and for different values of m. The results are coherent with the ones presented in the Tables 18 and 19. The monolithic and alternate linearized splitting solvers show clear improvements thanks to the AA, for both $m = 1$ and $m = 2$. For the nonlinear splitting solver, the AA does not seem to produce any improvement, as the rates of convergence seem to be the same. The result does not directly contradict the ones presented in the Tables 18 and 19; it simply states that, at the final time step, the AA does not produce any improvement. On the full simulation, we could observe a clear reduction in the numbers of iterations.

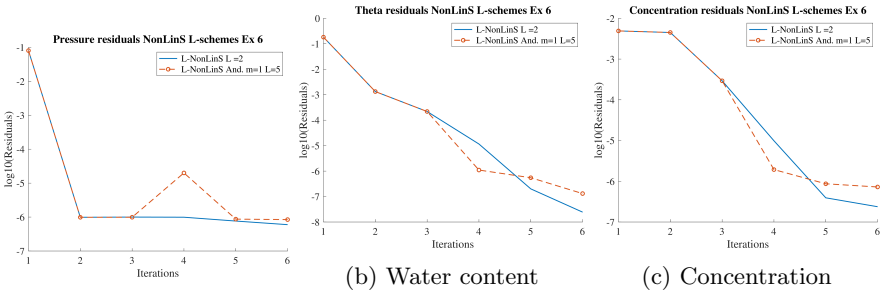

(a) Pressure residuals.

(b) Water content residuals.

(c) Concentration residuals.

Fig. 11.: Example 5: Residuals of each unknown at the final time step, NonLinS L-scheme. Here, different L and m are tested, $dx = 1/10$, and $\Delta t = T/25$.

Table 21 presents the precise rates of convergence of the different linearization schemes. Once more we can observe as the AA improves the rates of convergence of the solvers based on the L-scheme.

	Ls Mono	Ls NonLinS And.	Ls NonLinS	Ls NonLinS And.	Ls AltLinS	Ls AltLinS And.
Ψ	0.93	1.60	0.99	1.21	0.99	1.58
c	0.95	1.72	0.89	1.52	0.97	1.61
θ	1.08	1.69	0.94	1.07	0.99	1.10

Table 21: Example 5: Order of convergence of the linearization schemes.

4. CONCLUSIONS

We consider models for flow and reactive transport in a porous medium. Next, to account for the influence of the solute concentration on the flow parameters, we incorporate effects like dynamic capillary pressure and hysteresis. The problem results being fully coupled.

For solving the time discrete equations (9), obtained after applying the Euler implicit scheme, we investigate different approaches: a monolithic solution algorithm and two splitting ones. Furthermore, for solving the nonlinear problem, two linearizations are studied: the Newton method and the L-scheme. The latter appears to be more stable than the former, which is more commonly implemented.

Finally, we have studied the effects of the Anderson acceleration. We observed that its implementation is particularly simple and can result in significant improvements. There were cases in which the differences between the accelerated and non-accelerated schemes were minimal, but due to its simplicity and the possibility of the great reduction in the numbers of iterations, we think it should always be tested. Particularly, one can either invest time in finding the optimal L parameters or the best depth m for which the AA results in the fastest scheme. Often, finding the most suitable m is simpler, and it can results in impressive improvements.

References

[1] I. Aavatsmark, *An introduction to multipoint flux approximations for quadrilateral grids, Computational Geosciences Volume 6, Issue 3-4, Pages 405-432*, 2002.

[2] E. Abreu, J. Vieira, *Computing numerical solutions of the pseudo-parabolic Buckley Leverett equation with dynamic capillary pressure, Mathematics and Computers in Simulation, Volume 137, Pages 29-48*, 2017.

[3] E. Abreu, P. Ferraz, J. Vieira, *Numerical resolution of a pseudo-parabolic Buckley-Leverett model with gravity and dynamic capillary pressure in heterogeneous porous media, Journal of computational Physics, Volume 411*, 2020.

[4] A. Agosti, L. Formaggia, A. Scotti, *Analysis of a model for precipitation and dissolution coupled with a Darcy flux, Journal of Mathematical Analysis and Applications, Volume 431, Issue 2, Pages 752-781*, 2015.

[5] G. Albuja, A. I. Avila, *A family of new globally convergent linearization schemes for solving Richards' equation, Applied Numerical Mathematics, Volume 159, Pages 281-296*, 2021.

[6] W. Alt, H. Luckhaus, *Quasilinear elliptic-parabolic differential equations, Mathematische Zeitschrift, Volume 183, Issue 3, Pages 311-341*, 1983.

[7] D. G. Anderson, *Iterative Procedures for Nonlinear Integral Equations, Journal of the ACM, Volume 12, Issue 4, Pages 547-560*, 1965.

[8] T. Arbogast, M. F. Wheeler, *A nonlinear mixed finite element method for a degenerate parabolic equation arising in flow in porous media, SIAM Journal on Numerical Analysis, Volume 33, Issue 4, Pages 1669-1687*, 1996.

[9] D. N. Arnold, F. Brezzi, B. Cockburn, L. D. Marini, *Unified Analysis of Discontinuous Galerkin Methods for Elliptic Problems, SIAM Journal on Numerical Analysis, Volume 39, Issue 5, Pages 1749-1779*, 2006.

[10] A. Arraras, F. J. Gaspar, L. Portero, C. Rodrigo, *Multigrid solvers for multipoint flux approximations of the Darcy problem on rough quadrilateral grids, Computational Geosciences, https://doi.org/10.1007/s10596-020-09979-w,* 2020.

[11] J. W. Barrett, P. Knabner, *Finite element approximation of the transport of reactive solutes in porous media. Part 1: error estimates for nonequilibrium adsorption processes, SIAM Journal on Numerical Analysis, Volume 34, Issue 1, Pages 201-227*, 1997.

[12] M. Bause, J. Hoffmann, P. Knabner, *First-order convergence of multipoint flux approximation on triangular grids and comparison with mixed finite element methods, Numerische Mathematik, Volume 116, Issue 1, Pages 1-29*, 2010.

[13] A.Y. Beliaev, S.M. Hassanizadeh, *A Theoretical Model of Hysteresis and Dynamic Effects in the Capillary Relation for Two-phase Flow in Porous Media. Transport in Porous Media, Volume 43, Issue 3, Pages 487-510*, 2001.

[14] M. Berardi, F. Difonzo, M. Vurro, L. Lopez, *The 1D Richards' equation in two layered soils: a Filippov approach to treat discontinuities, Advances in Water Resources, Volume 115, Pages 264-272*, 2018.

[15] M. Berardi, F. Difonzo, L. Lopez, *A mixed MoL-TMoL for the numerical solution of the 2D Richards' equation in layered soils, Computers & Mathematics with Applications Volume 79, Issue 7, Pages 1990-2001*, 2020.

[16] J. W. Both, K. Kumar, J. M. Nordbotten, F. A. Radu, *Anderson accelerated fixed-stress splitting schemes for consolidation of unsaturated porous media, Computers & Mathematics with Applications, Volume 77, Issue 6, Pages 1479-1502*, 2019.

[17] S. Bottero, S. M. Hassanizadeh, P. J. Kleingeld, T. J. Heimovaara, *Nonequilibrium capillarity effects in two-phase flow through porous media at different scales, Water Resources Research, Volume 47, Issue 10*, 2011.

[18] G. Camps-Roach, D. M. O'Carroll, T. A. Newton, T. Sakaki, T. H. Illangasekare, *Experimental investigation of dynamic effects in capillary pressure: Grain size dependency and upscaling, Water Resources Research, Volume 46, Issue 8,* 2010.

[19] X. Cao, I. S. Pop, *Two-phase porous media flows with dynamic capillary effects and hysteresis: Uniqueness of weak solutions, Computers & Mathematics with Applications, Volume 69, Issue 7, Pages 688-695*, 2015.

[20] X. Cao, I. S. Pop, *Degenerate two-phase porous media flow model with dynamic capillarity, Journal of Differential Equations Volume 260, Issue 3, Pages 2418-2456,* 2016.

[21] X. Cao, K. Mitra, *Error estimates for a mixed finite element discretization of a two-phase porous media flow model with dynamic capillarity, Journal of Computational and Applied Mathematics, Volume 353, Pages 164 - 178*, 2019.

[22] X. Cao, S.F. Nemadjieu, I.S. Pop, *Convergence of an MPFA finite volume scheme for two phase porous media flow with dynamic capillarity, IMA Journal of Numerical Analysis, Volume 39, Issue 1, Pages 512–544,* 2019.

[23] D. M. O'Carroll, T. J. Phelan, L. M. Abriola, *Exploring dynamic effects in capillary pressure in multistep outflow experiments, Water Resources Research, Volume 41, Issue 11*, 2005.

[24] M. Celia, E. Bouloutas, R. L. Zarba, *A General Mass-Conservative Numerical Solution for the Unsaturated Flow Equation, Advances in Water Resources, Volume 26, Issue 7, Pages 1483-1496*, 1990.

[25] D. A. DiCarlo, *Experimental measurements of saturation overshoot on infiltration, Water Resources Research, Volume 40, Issue 4*, 2004.

[26] V. Dolejsi, M. Kuraz, P. Solin, *Adaptive higher-order space-time discontinuous Galerkin method for the computer simulation of variably-saturated porous media flows, Applied Mathematical Modelling, Volume 72, Pages 276-305*, 2019.

[27] R. Eymard, M. Gutnic, D. Hilhorst, *The finite volume method for Richards equation, Computational Geosciences, Volume 3, Issue 3-4, Pages 256-294*, 1999.

[28] C. Evans, S. Pollock, L. G. Rebholz, M. Xiao, *A proof that Anderson acceleration improves the convergence rate in linearly converging fixed point methods (but not in those converging quadratically), SIAM Journal on Numerical Analysis, Volume 58, Issue 1, Pages 788-810*, 2020.

[29] H. Fang, Y. Saad, *Two classes of multisecant methods for nonlinear acceleration, Numerical Linear Algebra with Application, Volume 16, Issue 3, Pages 197 - 221*, 2008.

[30] W. G. Gray, S. M. Hassanizadeh, *Macroscale continuum mechanics for multiphase porous-media flow including phases, interfaces, common lines and common points, Volume 21, Issue 4, Pages 261 - 281*, 1998.

[31] M. van Genuchten, *A Closed-form Equation for Predicting the Hydraulic Conductivity of Unsaturated Soils, Soil Science Society of America Journal, Volume 44, Issue 5, Pages 892-898*, 1980.

[32] R. Helmig, *two-phase flow and transport processes in the subsurface: a contribution to the modeling of hydrosystems, Springer-Verlag*, 1997.

[33] E. J. Henry, J. E. Smith, A. W. Warrick, *Solubility effects on surfactant-induced unsaturated flow through porous media, Journal of Hydrology, Volume 223, Issues 3-4, Pages 164-174*, 1999.

[34] N. T. Hoa, R. Gaudu, C. Thirriot, *Influence of the hysteresis effect on transient flows in saturated-unsaturated porous media, Water Resources Research, Volume 13, Issue 6, Pages 992-996*, 1977.

[35] D. Husseini, *Effects of Anions acids on Surface Tension of Water, Undergraduate Research at JMU Scholarly Commons*, 2015.

[36] D. Illiano, I. S. Pop, F. A. Radu, *Iterative schemes for surfactant transport in porous media, Computational Geosciences, https://doi.org/10.1007/s10596-020-09949-2*, 2020.

[37] D. Illiano, I. S. Pop, F. A. Radu, *An efficient numerical scheme for fully coupled flow and reactive transport in variably saturated porous media including dynamic capillary effects, accepted author manuscript, Numerical Mathematics and Advanced Applications ENUMATH 2019, Lecture Notes in Computational Science and Engineering 139, https://doi.org10.1007/978-3-030-55874-1_55*, 2020.

[38] A. Karagunduz, M. H. Young, K. D. Pennell, *Influence of surfactants on unsaturated water flow and solute transport, Water Resources Research, Volume 51, Issue 4, Pages 1977-1988*, 2015.

[39] S. Karpinski, I. S. Pop, F. A. Radu, *Analysis of a linearization scheme for an interior penalty discontinuous Galerkin method for two-phase flow in porous media with dynamic capillarity effects, International Journal for Numerical Methods in Engineering, Volume 112, Issue 6, Pages 553-577*, 2017.

[40] R. A. Klausen, F. A. Radu, G. T. Eigestad, *Convergence of MPFA on triangulations and for Richards' equation, International Journal for Numerical Methods in Fluids, Volume 58, Issue 12, Pages 1327-1351*, 2008.

[41] J. Koch, A. Ratz, B. Schweizer, *Two-phase flow equations with a dynamic capillary pressure, European Journal of Applied Mathematics, Volume 24, Issue 1*, 2012.

[42] P. Knabner, S. Bitterlich, R. I. Teran, A. Prechtel, E. Schneid, *Influence of Surfactants on Spreading of Contaminants and Soil Remediation, Jager W., Krebs HJ. (eds) Mathematics — Key Technology for the Future. Springer, https://doi.org/10.1007/978-3-642-55753-8-12*, 2003.

[43] H. Li, M. W. Farthing, C. N. Dawson, C. T. Miller, *Local discontinuous Galerkin approximations to Richards' equation, Advances in Water Resources, Volume 30, Issue 3, Pages 555-575*, 2007.

[44] K.-A. Lie, *An Introduction to Reservoir Simulation Using MATLAB: User guide for the Matlab Reservoir Simulation Toolbox (MRST), SINTEF ICT*, 2016.

[45] F. List, F. A. Radu, *A study on iterative methods for solving Richards' equation, Computational Geoscience, Volume 20, Issue 2, Pages 341-353*, 2016.

[46] S. B. Lunowa, I. S. Pop, B. Koren, *Linearized domain decomposition methods for two-phase porous media flow models involving dynamic capillarity and hysteresis, Computer Methods in Applied Mechanics and Engineering, Volume 372, https://doi.org/10.1016/j.cma.2020.113364*, 2020.

[47] A. Mikelic, *A global existence result for the equations describing unsaturated flow in porous media with dynamic capillary pressure, Journal of Differential Equations, Volume 248, Issue 6, Pages 1561-1577*, 2010.

[48] J.-P. Milisic, *The unsaturated flow in porous media with dynamic capillary pressure, Journal of Differential Equations, Volume 264, Issue 9, Pages 5629-5658*, 2018.

[49] K. Mitra, I. S. Pop, *A modified L-scheme to solve nonlinear diffusion problems, Computers & Mathematics with Applications, Volume 77, Issue 6, Pages 1722-1738*, 2019.

[50] J. McClure, R. T. Armstrong, M. Berrill, S. Schluter, S. Berg, W. G. Gray, C. T. Miller, *Geometric state function for two-fluid flow in porous media, Physical Review Fluids, Volume 3, Issue 8*, 2018.

[51] N. R. Morrow, C. C. Harris, *Exploring dynamic effects in capillary pressure in multistep outflow experiments, Water Resources Research, Volume 41, Issue 11*, 2005

[52] R. Nochetto, C. Verdi, *Approximation of degenerate parabolic problems using numerical integration, SIAM Journal on Numerical Analysis, Volume 25, Issue 4, Pages 784-814*, 1988.

[53] O, Oung, S. M. Hassanizadeh, A. Bezuijen, *Two-phase flow experiments in a geocentrifuge and the significance of dynamic capillary pressure effect, Journal of Porous Media, Volume 8, Issue 3, Pages 247-257*, 2005.

[54] C. Paniconi, M. Putti, *A comparison of Picard and Newton iteration in the numerical solution of multidimensional variably saturated flow problems, Water Resources Research, Volume 30, Issue 12, Pages 3357-3374*, 1994.

[55] M. Peszynska, S. Y. Yi, *Numerical methods for unsaturated flow with dynamic capillary pressure in heterogeneous porous media, International journal of Numerical Analysis and Modeling, Volume 5, Pages 126-149*, 2008.

[56] A. Prechtel, P. Knabner, *Accurate and efficient simulation of coupled water flow and nonlinear reactive transport in the saturated and vadose zone - application to surfactant enhanced and intrinsic bioremediation, International Journal of Water Resources Development, Volume 47, Pages 687-694*, 2002.

[57] I. S. Pop, F. A. Radu, P. Knabner, *Mixed finite elements for the Richards' equation: linearization procedure, Journal of Computational and Applied Mathematics, Volume 168, Issue 1, Pages 365-373*, 2004.

[58] F. A. Radu, I. S. Pop, S. Attinger, *Analysis of an Euler implicit, mixed finite element scheme for reactive solute transport in porous media, Numerical Methods for Partial Differential Equations, Volume 26, Issue 2, Pages 320-344*, 2010.

[59] F. A. Radu, A. Muntean, I. S. Pop, N. Suciu, O. Kolditz, *A mixed finite element discretization scheme for a concrete carbonation model with concentration-dependent porosity, Journal of Computational and Applied Mathematics Volume 246, Pages 74-85,* 2013.

[60] T. F. Russell, M. F. Wheeler, *Finite element and finite difference methods for continuous flows in porous media, SIAM, Pages 35-106*, 1983.

[61] B. Schweizer, *The Richards equation with hysteresis and degenerate capillary pressure, Journal of Differential Equations, Volume 252, Issue 10, Pages 5594-5612*, 2012.

[62] M. Slodicka, *A robust and efficient linearization scheme for doubly nonlinear and degenerate parabolic problems arising in flow in porous media, SIAM Journal on Numerical Analysis, Volume 23, Issue 5, Pages 1593-1614*, 2002.

[63] J. E. Smith, R. W. Gillham, *The effect of concentration-dependent surface tension on the flow of water and transport of dissolved organic compounds: A pressure head-based formulation and numerical model, Water Resources Research, Volume 31, Issue 3, Pages 343-354*, 1994.

[64] J. Smith, R. Gillham, *Effects of solute concentration-dependent surface tension on unsaturated flow: Laboratory sand column experiments, Water Resource Research, Volume 35, Issue 4, Pages 973-982*, 1999.

[65] F. Stauffer, *Time dependence of the relations between capillary pressure, water content and conductivity during drainage of porous media, IAHR symposium on scale effects in porous media, Volume 29*, 1978.

[66] S. Sun, M. F. Wheeler, *Discontinuous Galerkin methods for coupled flow and reactive transport problems, Applied Numerical Mathematics Volume 52, Issues 2–3, Pages 273-298*, 2005.

[67] M. Vohralik, *A posteriori error estimates for lowest-order mixed finite element discretizations of convection-diffusion-reaction equations, SIAM*

Journal on Numerical Analysis, Volume 45, Issue 4, Pages 1570-1599, 2007.

[68] H. F. Walker, P. Ni, *Anderson Acceleration for Fixed-Point Iterations, SIAM Journal on Numerical Analysis, Volume 49, Issue 4, Pages 1715 - 1735*, 2011.

[69] X. Wang, H. A. Tchelepi, *Trust-region based solver for nonlinear transport in heterogeneous porous media, Journal of Computational Physics, Volume 253, Pages 114-137*, 2013.

[70] C. S. Woodward, C. N. Dawson, *Analysis of expanded mixed finite element methods for a nonlinear parabolic equation modeling flow into variably saturated porous media, SIAM Journal on Numerical Analysis, Volume 37, Issue 3, Pages 701-724*, 2000.

[71] Y. Zha, J. Yang, J. Zeng, C.-H. M. Tso, W. Zeng, L. Shi, *Review of numerical solution of Richardson-Richards equation for variably saturated flow in soils, WIREs Water, Volume 6, Issue 5*, 2019.

[72] H. Zhang, P. A. Zegeling, *A Numerical Study of Two-Phase Flow Models with Dynamic Capillary Pressure and Hysteresis, Transport in Porous Media, Volume 116, Issue 2, Pages 825-846*, 2017.